Global shifts in mountain wave turbulence within high resolution climate models.

Isabel H. Smith[1], Paul D. Williams[1], and Reinhard Schiemann[1,2]

[1]University of Reading, UK

[2]National Center for Atmospheric Sciences, UK

Correspondence: Isabel H. Smith (smith.isabel.helen@gmail.com)

Abstract. Using a multi-model approach, this paper ~~quantified~~ quantifies global changes in moderate or greater mountain wave turbulence (MWT) within a high-end warming scenario ~~. Initial results found model resolution dependency apparent, therefore~~ by 2050. We first show that simulated MWT changes depend on model resolution and therefore select three high resolution global climate ~~modelled datasets were used within the~~ model experiments for further analysis; HadGEM3-GC3.1-HM (25km), EC-Earth-3P-HR (36km) and MPI-ESM1.2-XR (34km). ~~Regional dependencies developed around each model and index, with seasonal components an important contributor to results~~At the regional scale, MWT change is found to depend on the climate model and MWT index used, as well as the season. A sub-continental approach was ~~developed~~used, focusing on all regions in which MWT ~~arose. On average, the North American continent projected an increase in MWT, but a~~ is seen in the model. MWT is projected to increase over North America as a whole but projected to decrease over the Rocky ~~Mountain range. This decrease was apparent in all seasons but northern hemisphere (NH) winter, with an increase of +60.6% over the 101 year investigation period. NH summer, spring and autumn dropped by -58.3%, -41.2 % and -30.9%. Over several mountain ranges an increase was evident, particularly over Greenland and regions in Asia. However, a drop in MWT also arose over~~ Mountains. An increase in MWT is projected for other regions including the Antarctic, Greenland, Georgia, Azerbaijan and parts of Chile and Argentina. A decline in MWT is projected for the Alps, Atlas and northern and central Andes. ~~Southern Andes and the Himalayas had seasonal differences resulting in a mix of projected outcomes. A final aim arose around the connection to low-level, surface wind flow~~ We also explore the modelled relationship of 10m wind speed and MWT production~~. This paper found links between MWT trends and the shift in projected median surface wind flow~~; there is a positive correlation between the projected changes of MWT and surface wind speed. The aviation sector should be aware of the future projections in MWT, particularly for ~~those were large increase over the 101 year period were evident~~regions where a large increase in MWT is projected, such as ~~Asia, Greenland and the Antarctic~~ the Antarctic and Greenland.

Mountains have a large impact on the atmosphere, from increasing localised precipitation events, to ~~generating vertical and horizontal atmospheric~~ the generation of vertically and horizontally propagating atmospheric gravity waves. Mountain waves can grow, as they propagate into higher altitudes with lower air density (Kim et al., 2018), steepen and eventually overturn breaking down into turbulent flow. This breakdown ~~develops typically lower at the tropopause. This boundary,~~ can develop around the tropopause, a boundary between the troposphere and stratosphere ~~, is a region of~~ with enhanced turbulent mixing ~~, with~~ of ozone, water vapour and aerosols exchanged between both layers (Whiteway et al.,2003; ~~lane et .al~~Lane et al., 2009). ~~This height is also a typical cruising altitude for the aircraft, a part~~ The tropopause (9-17km above the surface) is a height often used by cruising aircraft. The cruising segment is a phase of the flight ~~in which passengers and on-board crew are more likely not to be wearing their seat belts~~ where passengers and crew are commonly not wearing seatbelts (Kim et al., 2018). This type of ~~upper level~~ upper-level turbulence is referred to as Mountain Wave Turbulence (MWT). MWT is the most significant mechanisms that impacts aircraft safety near mountains (Lane et al., 2009). ~~Atmospheric~~ In general, atmospheric turbulence has a dangerous and damaging cost on the aviation sector. Delays, injuries and fatalities have a huge economic loss worth millions of US dollars a year (Wolff and Sharman, 2008). ~~An aircraft caught in a patch of turbulence has to quickly change altitude. This leads to substantial shift in airspeed, which increases the chance of a system stall (Sharman and Pearsons, 2017).~~ Types of upper-level turbulence are defined by the features which develop them, for example turbulence that develops in vertically deep convective cloud is referred to convectively induced turbulence (CIT) (Wolf and Sharman 2008). MWT, unlike in-cloud CIT, is not detectable by on-board RADAR equipment (Sharman and Lane, 2016). ~~Therefore flights can be struck suddenly which can lead~~ Here CIT relates to in-cloud formation, not near-cloud turbulence (NCT) which cam develop from 5 to 200 kms away from active convective systems (Chun and Kim, 2008). MWT can impact a flight with little warning, leading to serious injuries and damages. Clear Air Turbulence (CAT), coined due to its formation without any convective features, is also not delectable. CAT often forms in the presence of an upper level frontal system, a jet core or jet stream. MWT ~~is~~ and NCT are often included within CAT, due to ~~its~~ their cloud-free, stratified development ~~.~~ (Clark et al., 2000).

Global ~~troposheric~~ tropospheric warming has an impact on the frequency of CAT production in both observations and projected ~~modeled~~ modelled data, with a global increase concluded in several studies (Williams and Joshi, 2013~~;~~ ; Storer et al. 2019, Kim et al., 2023; Prosser et al., 2023; ~~Storer~~ Smith et al.~~2019 and Smith~~ , 2023; Foudad et al.~~2023). Upper level~~ , 2024). Upper-level jet streams are shifting in speed and momentum with global temperature gradients altered, resulting in an increase in CAT production. However, new areas of research are trying to quantify the impact of global warming on MWT. Any future change to MWT will be equated to a shift in low level wind speed or a change in upper-level dynamical features suppressing or energising the breaking of inertial gravity waves. Kim et al. (2023), using a high-end SSP climate scenario, investigated the change in MWT between 1970-2014 and 2056-2101. Their paper used 14 different diagnostics to represent MWT within model data, with several indices and regions projecting an increase in the probability of encountering strong turbulence. The regions with a decline in MWT ~~,~~ also had near-surface winds projected to ~~also~~ weaken in time. Observations have shown a global slowing in surface winds over previous decades, ~~refereed~~ referred to in literature as terrestrial stilling (TS). Despite TS shifting with several modes of climate variability (Zeng et al, 2019), it is projected to continue in many areas of the globe, including the northern hemisphere (NH) mid latitudes, in both middle to high warming projections (Deng et al., 2022). Kim et al. (2023) overall found an increase in MWT over two thirds of the globe, with large variations over the tropical regions.

Global climate models (GCM) are commonly used to investigate the changes in CAT and MWT in time (Williams and Joshi, 2013; Storer et al. 2019, Kim et al., 2023; Prosser et al., 2023; Smith et al., 2023; Foudad et al., 2024; Kim et. al, 2023), with GCMs turbulence representation in the atmosphere as capable as re-analysis data (Williams and Storer, 2022). The spatial and temporal resolution in a GCM is an advantage, compared to, for example, verbal pilot reports (PIREPS). Aircraft encountering turbulence are required to record the time, location and severity of the event ~~. These reports are referred to as PIREPs. PIREP~~ (PIREPs). PIREPS datasets are effective for turbulent climatology research but are not always reliable in their location or timing (Gill and Buchanan, 2018), with median uncertainties of around 50km horizontally, 70m vertically and 200s temporally out (Sharman et al., ~~2006).Many previous studies, investigating trends in atmospheric turbulence, have used global climate models (GCMs)over PIREPs. Williams and Storer (2022) found GCMs can effectively represent turbulence in the atmosphere as well as re-analysis data.~~ 2014, Sharman et al., 2006). The latest phase of ~~the~~ Coupled Model Intercomparison Project (CMIP6) has a subsection of high resolution ~~global climate models~~ GCMs (HighResMIP) ~~. This subsection was developed to bridge the~~ developed purely to investigate global meteorological dynamical processes and to bridge the resolution gap between numerical weather predictions ~~grid spacing sizes and GCMs, and to investigate global meteorological dynamical processes in higher resolution~~ (NWP) and climate models (Haarsma et al., 2016; Smith, et al. ~~–~~, 2023). ~~This paper aims to understand if MWT is projected to change within CMIP6 HighResMIP modelsover a 101 year period starting in 1950 and ending in 2050, using some indices applied~~ To test the capability of these HighResMIP models, and to add to Kim et. al (2023), our project explores global and seasonal MWT trends between 1950 to 20250, and the uncertainties and differences that can arise using a multi-model approach. Due to the surface wind speed findings in Kim et. al (2023)~~. Also, we aims to understand if resolution is important for capturing MWT~~, ~~if CMIP6 models project TS and if TS differences globally result in changes to MWT~~we too explore if shifts in wind speeds are the cause of projected MWT variations over the 101-study period. The layout of this paper entails a methodology section, which details the models and indices used to diagnose MWT, and all data processing techniques, the results section and finally concluding remarks. The model and index uncertainties are highlighted in the continental analysis in section 3.2 of the results, with a multi-model and index mean used for sub-continental, mountain range dependent analysis (section 3.3). ~~A final aim is to understand seasonality variation in MWT changes.~~

2 Methodology and Data

2.1 CMIP6 HighResMIP global climate models

MWT is difficult to forecast, with the theory very well understood, but ~~capacity to resolve the wave-length of inertial gravity waves and the turbulent kinetic energy difficult~~ difficult to capture due to its small scale nature (Gill and ~~Striling, 2013). One can assume~~ Stirling, 2012). Within this paper, we make the assumption that large scale eddies will eventually cascade down the inertial sub-range into micro-scale sizes and into turbulent kinetic energy (Lester~~1993,~~ , 1993; Sharman and Lane, 2016)~~. This assumption allows investigations to use data with~~ , allowing us to use a range of ~~resolutions. CMIP was set up in the 1990s to evaluate, collate and improve GCMs . Simulations from three CMIP6-HighResMIP GCMs are used in this study.~~model resolutions for this investigation. Our investigation uses a multi-model approach with 3 GCMs spanning 7 horizontal grid size domains. All models are part of CMIP6 HighResMIP simulations (Haarsma et al., 2020). These GCMs are HadGEM3-GC3.1 , with ~~three grid spacing~~ 3 domains available (-HM; 25km, -MM; 60km, -LL; 135km) ~~,~~ (Roberts et al., 2019), MPI-ESM1.2 with ~~two~~ 2 domains (-XR; 34km, -HR; 67km) (Gutjahr et al., 2019) and EC-Earth with ~~two~~ 2 domains (-3P-HR; 36km , -3P; 71km) ~~.~~ (Haarsma et al., 2020). The finer sub-models may start to resolve patches of turbulence, which ~~are~~ climatology suggests are around 60km wide and 1km deep (Sharman et al., 2014). Due to this 1km vertical depth, we focus on the model horizontal resolution, with thickness representation currently unattainable on our modelled vertical levels. These finer horizontal resolutions are used for the majority of the paper, discussed further in section 3.1. This study uses the historically forced coupled climate and ocean experiments (1950-2014) with the future projected forcing of 2015–2050, simulating the high end SSP8.5 scenario (Haarsma et al., 2016).The benefits of using these CMIP6 GCMs relates to the global variability of our data, and the finer spatial resolution (relative to other global models). There are some limitations such as the smoothed topography limiting our ability to detect the complex MWT generation. This limitation means that not all MWT prone zones, found through observations, are detected by our approach (Fig. 1). This issue is also related to our dependency on terrain gradient discussed next. Our approach is done to explore the capability of our models, but future work could apply NWP modelled terrain to quantify further complexities.

2.2 Diagnosing turbulence

To diagnose regions of turbulence, a number of indices, linked closely to atmospheric instability, are applied to our CMIP6 GCMs ~~data~~simulations. MWT and CAT share similarities in their formation, so previous literature has applied CAT indices to represent MWT in the atmosphere. Sharman and Pearsons (2017) and Kim et al.(2023) combine CAT diagnostics with certain surface and terrain variables to create an index that just ~~diagnoses~~ represents MWT;

$$Index_{MWT} = Index_{CAT} * Ds$$

Ds is ~~the~~ a non-zero near-surface element that's model and index dependent. Within this paper, Ds = surface height (>200m) multiplied by both terrain gradient (>0.5 km m^{-1}) and ~~surface wind speed .~~ maximum low-level wind speed (<1km). Ds values differ across each model, with terrain gradient model dependent. Sharman and Pearsons (2017) determined, through experimentation, that these three variables within Ds combined with a CAT diagnostics represented MWT effectively. Kim et al. (2023) tested using vertical velocity within Ds, instead of low-level wind speed, but found a poorer statistical evaluation. ~~Terrain gradient is an important quantity with its association with linear gravity wave theory, and the wave of a gravity wave amplitude being proportional to the terrain slope magnitude (Wolf and Sharman, 2008).~~ This method of calculating MWT was deemed skilful against PIREP data, in comparison to a orthographic gravity wave parametrisation scheme (Kim et al., 2018). In our study, we apply six indices used previously to diagnose the presence of CAT (Williams, Joshi (2014). These CAT indices are ~~Horizontal~~ horizontal temperature gradient (HTG), ~~Frontogensis~~ frontogenesis function (FF), the divergence of horizontal wind (DIV), 200hPa wind speed (WS), flow deformation (FD) and finally a combination of flow deformation and wind speed (FDWS). Each MWT index is denoted with the subscript of their CAT index contributions, for example MWT_{HTG} is the product of ~~Horizontal temperature Gradient~~ horizontal temperature gradient and Ds. Sharman and Pearsons (2017) found that these 6 indices, with 8 others, are very well at representing MWT at high altitudes ~~with an area under the curve (AUC) of 0.989 within Receiving operating curve (ROC) analysis. Horizontal Temperature~~ and particularly good at avoiding false alarms situations, with a probability of detection for non-events (PDON) at 98.9%. Horizontal temperature gradient (combined with Ds) ~~also was found to pick up MWT effectively with an AUC of 0.991. These results have only been tested over~~ on its own also has a PDON 99.1%. However, Sharman and Pearson (2017) only focuses on the contiguous united states of America (CONUS). ~~Our~~

Following recent MWT literature (Kim et al., 2023), our study assumes moderate or greater (MOG) turbulence is arising globally at the 98th percentile value of each index ~~, following recent MWT literature (Kim et al., 2023)~~ and focuses on the atmospheric pressure of 200 hPa (native vertical levels from projections). These threshold values are index but also model, and ensemble member dependent. Further information found within Appendix B.To statistically determine the change in projected MWT, our results use a linear regression fit, with a confidence interval of 95%. Trends that do not meet this confidence interval are removed from the multi-model and index averages. As an extra research question, this paper looks at the average and maximum 10m wind speeds for participial regions to explore TS in our models. Since our analysis is related to the change in MWT over the century, using both the average and maximum helps equate the general trend in time (average) and if there are more instances of rapid wind speeds that lead to further MWT generation (maximum).

~~Low-level wind speed is a variable considered on its own within this paper.The variations in the maximum and median values in wind speed are investigated separately. This method was determined to understand on average how surface wind flow is changing, and if this change is also found in the high-end maximum wind flow.~~

Figures/MWT_figures/MWT_Over_Globe.png

Figure 1. Areas of the globe in which our GCMs project MWT, averaged over three GCMs; HadGEM3-GC3.1-HM, MPI-ESM1.2-XR and EC-Earth-3P-HR, across all indices; MWT_{FD}, MWT_{FDWS},MWT_{WS}, MWT_{HTG}, MWT_{FF},MWT_{DIV}.

3 Results and Discussion

As discussed, terrain height and gradient are applied to CAT indices to identify MWT. The importance of terrain gradient is highlighted effectively in ~~figure 1. This figure shows the regions of the globe where our indices diagnose~~ fig. 1, which portrays the areas where our models diagnosed MWT. Regions of the globe with large plateaus, such as Greenland and the Tibetan Plateau, are enclosed by areas of MWT with these steep slopes dominating. As expected, MWT is most prominent over large mountain ranges, such as the Andes, Rocky and Himalayas.

3.1 Two ~~Decade Comparison~~decade comparison

The MOG MWT decadal difference between 1950-60 and 2040-50 are displayed within ~~figure 2 .~~ fig. 2. Here this relative change in MWT is shown for all models domain sizes averaged across the six indices. A definitive lack of detail is evident within mid-range/coarser sub-models, clearly shown by HadGEM3-GC3.1-LL (~~figure~~ fig. 2i) with few MWT zones. ~~Previous~~ PIREP analysis suggests that there are considerable more regions where aircraft have experienced MWT ~~,~~ (Sharman et. al, 2014), for example North America projected MWT is non-existent within this 135km grid spaced model. ~~For MWT , a resolution dependence has arisen.~~ Our coarser models fail to represent MWT in several locations, with a key limiting attribute our terrain gradient threshold and the unfortunate smoothing of terrain implemented in climate models. This creates a model resolution criterion for our MWT analysis. It may differ in other studies that imported terrain from a NWP model, but our study is to highlight the uncertainties on representing MWT in GCMs. Interestingly, the mid-range sub-models project similar MWT changes, when compared to their finer counterparts. This is shown effectively within subplots (2g) and (2h), which display the average across the models, regridded to 36km and 71km respectively. Both subplots have a separate steep increase or decrease over Greenland and northern South America. However, there are differences in the amount of "white" patches, which simply project "no-change" but the occurrence of MWT. The agreement across model resolutions, adds weight to the confidence in MWT projections, however, due to the increase detail in fine grid domain models, this paper progresses with the three finer models shown in ~~figure~~ fig. 2.a, 2.c, 2.e.

3.2 ~~Seasonality of~~ Continental index and model variability in seasonal MWT ~~; yearly analysis~~projections

~~Due to the range of results from the decadal comparison, fig's 3-9 separately display indices individually~~

This section explores the variability in the three modelled projections, and the MWT index uncertainty, over each continent (fig. 3-9). For clarity, insignificant linear regression trends (less than a 95th confidence level) within season or model are greyed out of figure legends. All four season are individually processed, with a final annual yearly median taken and plotted. As expected, all annual averages reside in the middle of their seasons. These results focus on the change each year in MWT compared to a global threshold for MOG (~~98~~ 98th percentile) turbulence found using all years (and seasons) with the 1950-60 decade. Using a global threshold provides information on the most turbulent

Figures/MWT_figures/Over_all_resolutions.png

Figure 2. Decade difference in MWT between 1950-59 and 2040-49, for all seven resolutions; HadGEM3-GC3.1-HM 25km,-MM 60km (a,b),-LL 135km (i), EC-Earth-3P-HR 36km,-3P 71km (c,d)and MPI-ESM1.2-XR 34km, HR- 67km (e,f). Subplots g,h show average across finer and mid-range GCMs. Conservative regridding method, modifying data into 36km and 71km across the finer and mid-range domains.

projected regions of the globe, ~~most~~ evident through analysis of the y-axis in all subplots in aforementioned figures. ~~In order of most turbulent, Asia, South America, the Antarctic, North America, Africa, Europe and the Australian continent y-axes range from +75 to +275%, 0 to +250%, -50 to 250 %, 0 to +100%, -100 to +60%,-60 to 20% and -95 to -75% respectively. Interestingly, the larger spread highlights differences across the indices and the seasonality of MWT, with winters and summers in both hemispheres characterised with the maxima in MWT in majority of cases. The slopes of the linear regression lines, in figure 3 to 12 (and in section 3.3), are the percentage trend in time per year. However, averaging over an entire continent has lead to a wide spread of results, and in multiple cases has lead to slope errors greater than the absolute slope value. Implying, at a 95% confidence level, that time has no significant linear effect on MWT, with slopes not statistically distinguishable from zero. The percentage of significant trends in each figure is presented in Table 1 and 2, highlighting the variability within the models and lack of confidence in some GCMs. Averages within such tables only include significant slopes.~~

3.2.1 North America

This paper includes Greenland within North America. ~~However, it should be noted that~~ Greenland has large increases in MWT, evident in ~~figure~~ fig. 2 to ~~5~~ 3 and within Section 3.3 where it is discussed further. This may skew an increase in MWT within this sub section, with variability across North America previously shown. ~~Seasonal difference in MWT amounts are evident~~ There are seasonal differences in the amount of projected MWT in North America, with ~~percentage changes in winter propagating at higher y-axis values within figure~~ a comparably large amount in DJF (December, January, February) within fig 3's HadGEM3-GC3.1 and EC-Earth-3P subplots. This is expected ~~,~~ with NH winter favourable for MWT generation over USA and Canada, with lowered tropopause heights and peak surface westerlies crossing mountain ranges perpendicularly (Guarino, et al. 2018). ~~Fascinatingly,~~ MPI-ESM1.2 ~~has DJF (December, January, February)~~ DJF and SON (September, October, November) ~~propagate at similar values~~ projections are similar in MWT_{FD}, MWT_{FDWS}, MWT_{WS} within ~~figure~~ fig. 3, with DJF at times below that of SON and other seasons. A double peak in maxima has been shown in some climatology MWT North America studies. Wolff and Sharman (2008), using PIREP data to find trends in MWT on the United States of America, found peaks in ~~meteorological NH's winter and spring~~ DJF and NH spring (MAM; March, April, May) but not necessarily ~~autumn~~SON.

~~A large number of insignificant trends arose across~~ Over North America, ~~with MWT $_{HTG}$'s annual, DJF, JJA (June, July, August) results projecting too much variability to definitive show any change in time any of the GCMs. A similar outcome for MWT_{DIV}, with only two slopes projecting a significant trend (EC-Earth-3P annual and HadGEM3-GC3~~our three high resolution models agree strongly that MWT has increased over the 101-year period, with an average over all seasons at 0.063 %/yr, 0.05 %/yr and 0.046 %/yr for HadGEM-GC3.1-HM~~SON). Across this continent, only 44 lines, out of 90, project significant trend. Within Table 1, the percentage of slopes, deemed to be significant, within North America are 61.11 %, 33.33 %, 22.22 %, 55.56 % and 72.22% across the entire year, DJF,~~

MAM , JJA and SON respectively. Its evident that the overall annual value is brought up by the higher percentage of confident slopes in SON. Although within Table 1, , EC-Earth-3P-HR median in SON is 0.013 +/- 0.034 %/year. This large error occurs due to the range of confident trends, with MWT$_{FDWS}$ and MWT$_{HTG}$ projecting a significant decline but other indices projecting a rise in MWTfrequency. Table 1 further displays an overall average increase in MWT over North America, with only these two indices projecting negative slopes in NH autumn. These negatives are highlighted in the range row within Table 1, with SON projecting a change of -4.3 to 16.3% over the 101 year period. Annual, DJF, MAM and JJA return similar ranges within the positive spectrum of 2.4 to 9.5 %, 3.7 to 13.0 %, 3.5 to 8.5% and 2.9% to 10.7%.

NH SON results, on average over the North America continent, have the largest high end positive increase in MWT with the greatest and MPI-ESM1.2-XR. These slopes, and other for each season and continent can be sourced from Table 1. This projected increase in MWT was evident in all but two indices, with MWT$_{HTG}$ and MWT$_{FDWS}$ SON projecting a drop in MWT. Apart from these two slopes there is good agreement across the indices and a similar trend across seasons. There are some seasons that have a greater number of significant slopes and the greatest low end projected drop in MWT. On average, SON is projected to increasein MWT by 8.1% from 1950 to 2050. MAM, JJA, DJF and annual on average across this period project a rise by 7.2%($p<0.05$) than others. For example, North America MAM only has 4 significant slopes, whereas SON has 13 (11 increase, 7.0% , 6.4% and 3.3%, individually2 negatives; Table 1) and the largest average slope of 0.08%/yr which equates to 8.08% over the projected period.

3.2.2 South America

The annual and seasonal percentage changes in MWT over South America are displayed in figure fig 4. The Index variability is clearly visible within this figure (y-axis ranging from 0 to 250 %, highlights differences in diagnostics projections, with MWT$_{FF}$ projecting rates that are also found in Asia and the Antarctic (figure 7 & 12). In contracts, EC-Earth-3P-HR's MWTspread), with MWT$_{FDWS}$ (figure 4.n) propagates at values are much smaller, similar to rates within Europe and Africa projections(figure 5 & 9). Most other diagnostics propagate values around the 0-50% range and MWT$_{FF}$ around the 180-250% range (4.d-f). This means the indices project a different amount of MWT over the region and are not capturing similar MWT generation situations. This is not an issue, as the purpose of using 6 indices is to capture the many situations in which MWT may occur, but interesting that this is evident within the South America projections. The remaining diagnostics sit at around +100%, although there are clear seasonal variations, with SH winter the most turbulent season for all diagnostics, expect MWT$_{FF}$. In comparison to North America, South America projections have a higher number of significant slopes with 61/90 (67.7%). However, this rate is not evenly spread across the indices. Within figure 4, . This is an index variation, rather than a model disagreement, with all models preforming similarly.

However, models do differ on trends over the period, for example MWT$_{HTG}$ decreases in HadGEM-GC3.1-HM (4.a) but increases in EC-Earth-3P-HR (4.b) and in MWT$_{FD}$ only has five (out of 15) significant trends, with three in MPI-ESM1.2-XR (annual, DJF and JJA) and two in HadGEM3-GC3$_{FDWS}$ there is a decreases in HadGEM-GC3.1-

Line plots of relative percentage change over North America for each year and season compared to a 1950 decadal global references, for each GCM; HadGEM3-GC3.1-HM, EC-Earth-3P-HR, and MPI-ESM1.2-XR and for each individual index. Line colour and marking differ for each season, with DJF blue and dashed, MAM green and dash dotted, JJA red and soild, SON purple and dotted. Annual change, which includes all seasons is black and solid.

Figures/MWT_figures/North_America.png

Figure 3. Line plots of relative percentage change over North America for each year and season compared to a 1950 decadal global references, for each GCM; HadGEM3-GC3.1-HM, EC-Earth-3P-HR, and MPI-ESM1.2-XR and for each individual index. Line colour and marking differ for each season, with DJF blue and dashed, MAM green and dash dotted, JJA red and soild, SON purple and dotted. Annual change, which includes all seasons is black and solid.

HM (JJA and SON) . Within JJA, MWT$_{FDWS}$, MWT$_{WS}$ and MWT$_{HTG}$ only have one model each projecting a significant trend. Within Table 1, DJF and annual have a much higher percentage of confident slopes, with 83.3 and 88.9%.

The average over all GCMs across the 4.m) and MPI-ESM1.2-XR (4.o) yet an increases again in EC-Earth-3P-HR (4.n). The projected trends, over South America, displayed with Table 1, are interestingly dominated by negatively sloped projections. This suggests a decline in MWT over the period. However, EC-Earth-3P-HR projections often counter this with a rise in MWT frequency. If all three GCMs produced a similar trend (a) and had all indices agreeing, differ across the seasons, models and indices. On average, a decrease in MWT is projected for South America, with the largest decline (with a high number of significant slopes(b), theoretical weight would be added to the projected outcome. Despite several indices having two or three GCMs meeting condition b) , condition a) is met less often in this continent. HadGEM3-GC3.1-HM and MPI-ESM1.2 suggests a decline in MWT in most indices over all seasons and annually in South America. Although there are four positive slopes in the Met. Office Hadley centre model (HadGEM3-GC3.1-HM) , for MWT$_{FD}$'s JJA and SON and MWT$_{FF}$'s MAM and JJA projections. All indices in the EC-Earth GCM project an increase in MWT apart from MWT$_{WS}$ which displays a decline annually, in DJF and JJA. Section 3.1 determined the largest differences in results between the indices, rather than GCMs. Here a regional dependency is introduced, with South America having larger model disagreement rather than index variation. slopes, 13:2) in DJF (SH summer) by 0.044 %/yr or 4.44% over the period.

3.2.3 Europe

Figure There are lower MWT rates over Europe compared to the global thresholds used, and so fig. 5's results, which show the change in MWT compared to a global threshold over Europe, propagate below the zero-y-axis line for the majority of the period. This means that this region of the globe has less MWT within the GCMs than the global average. However, DJF values, in many indices, crosses into positive percentage changes, making it a more turbulent season. Interestingly, EC-Earth-3P-HR's MWT$_{HTG}$ and MWT's plots mostly reside within the negative y-axis, although some DJF projections filter into the positive side. The projected trends in Europe are index dependent, despite strong model agreement (excluding MWT$_{FDWS}$have spring at a similar propagating level. Almost all MWT; 5.m-n). This leads to competing slopes and low overall-multi-model projections. All seasons too agree in a certain trend, with a positive or negative slope all index dependents. The number of confident slopes is relatively small compared to the other continents with only one index (MWT$_{HTG}$lines are significantly sloped, but one in JJA.

~~Line plots of relative percentage change over South America for each year and season compared to a 1950 decadal global references, for each GCM; HadGEM3-GC3.1-HM, EC-Earth-3P-HR, and MPI-ESM1.2-XR and for each individual index. Line colour and marking differ for each season, with DJF blue and dashed, MAM green and dash dotted, JJA red and soild, SON purple and dotted. Annual change, which includes all seasons is black and solid.~~

Figures/MWT_figures/South_America.png

Figure 4. Line plots of relative percentage change over South America for each year and season compared to a 1950 decadal global references, for each GCM; HadGEM3-GC3.1-HM, EC-Earth-3P-HR, and MPI-ESM1.2-XR and for each individual index. Line colour and marking differ for each season, with DJF blue and dashed, MAM green and dash dotted, JJA red and soild, SON purple and dotted. Annual change, which includes all seasons is black and solid.

Overall, this index projects a decline in MWT in all seasons , at most by -0.177%/year in SON, a decrease of 18% over the period. MWT_{DIV}, also projects a decline but DJF or MAM cannot be included in overall analysis with considerable slope error.

However, MWT_{FF}, MWT_{FD} and MWT_{WS} all project an increase in their significant slopes. The remaining index , MWT_{FDWS}, has opposing signs across GCMs with HadGEM3-GC3.1 suggesting an increase with the previous three indices and EC-Earth-3P-HR projecting a reduction in MWT. ; 5.c) significant in MPI-ESM1.2has no significant slopes within this index. As evident from Table 1, when averaging across this figure, DJF, MAM and annual project an increase of 0.043, 0.057 and 0.039 %/year. An almost opposite response apparent in SON, with -0.045 % per year. JJA has too much variability to show any clear response. Like South America, Europe did not meet condition a) but it also did not meet condition b), with large variations across both models and indices, suggesting a less confident response. -XR projections. Summer in Europe (JJA) had the highest relative percentage of significant slopes with a decline average of -2.323 %. by the end of the 101-year period.

3.2.4 Africa

Figure 6 displays the percentage change in MWT over the African continent. The most notable result within this figure is the level on the y-axis that HadGEM3-GC3.1's MWTAs the situation in South America, but at a different range, indices differ in the amount of MWT projected over Africa (fig.6) , with -75% in MWT_{FDWS} , -50% in MWT_{FD}, -25% in MWT_{WS}, MWT_{DIV}, MWT_{FDWS} and +50% in MWT_{FF} lines propagate at . This height on the on the y-axisis comparable with the amount of turbulence over North America. This index previously projected relatively large percentage changes, compared to the other five indices, in section 3.2. The amount of projected MWT in Africa is similar to that in Europe. For trends over the period, like Europe, a general decrease in MWT develops, however with more confident negative slopes. A clear decline in DJF, JJA and SON with a mix in MAM. Strong model agreement within this continent, with largest variation due to index differences. It should be noted that strong model agreement is only between EC-Earth-3P-HR and HadGEM-GC3.1-HM, with MPI-ESM1.2over South America. Most indices in Africa reside in the negative spectrum, with the amount of MWT turbulence similar to Europe or below. One index of interest, when considering the trend of the data, is MWT_{DIV}. All three GCMs agree, all with significant slopes, that MWT, diagnosed by MWT_{DIV}, is decreasing over Africa in all seasons. The remaining 5 indices do not have all three GCMs producing significant slopes or have them agreeing on a trend. There are multiple indices that do agree with the decline in JJA, SON, DJF and annually, as seen by the overall

~~Line plots of relative percentage change over Europe for each year and season compared to a 1950 decadal global references, for each GCM; HadGEM3-GC3.1-HM, EC-Earth-3P-HR, and MPI-ESM1.2-XR and for each index. Line colour and marking differ for each season, with DJF blue and dashed, MAM green and dash dotted, JJA red and soild, SON purple and dotted. Annual change, which includes all seasons is black and solid.~~

Figures/MWT_figures/EUROPE.png

Figure 5. Line plots of relative percentage change over Europe for each year and season compared to a 1950 decadal global references, for each GCM; HadGEM3-GC3.1-HM, EC-Earth-3P-HR, and MPI-ESM1.2-XR and for each index. Line colour and marking differ for each season, with DJF blue and dashed, MAM green and dash dotted, JJA red and soild, SON purple and dotted. Annual change, which includes all seasons is black and solid.

~~average decrease in such seasons in Table 1. However, MAM has a wide range of significant slopes, and overall ends up projecting a positive trend of~~ -XR results all insignificant. This could be due to the number of ensemble members within this simulation. As mentioned in our methods, only 1 ~~% over the 101 years~~ensemble for this run is used.

3.2.5 Asia

Due to the Himalayan Mountains and many other steep mountain ranges over Asia, the MWT percentages on the y-axis in ~~figure~~ fig. 7 are the largest compared to any other continent. The seasonality of MWT is very interesting over Asia, with different indices projecting MAM, JJA or DJF to have the maxima in MWT across their retrospective subplots. ~~In section~~ Further explored in our regional analysis (section 3.3~~, regional analysis should help further understanding on the mix of seasonal maximums~~). Interestingly, ~~MWT$_{FF}$ again projects the largest percentage change ranges within figure 7 . In this case many other indices are propagating at a percentage value near or just below this index, adding confidence in the high amount of MWT over Asia.~~

~~As shown by slopes in figure 7 and Table 2,~~ MPI-ESM1.2-XR projection are all around 150% (y-axis) no matter the index, whereas there's a wider spread across the seasons and indices for the remaining models. In terms of trends over the period there is a mix ~~in projected trends for MAM and SON. Within MAM results,~~ depending on season, index and model. For MWT$_{HTG}$~~and MWT~~, strong model agreements that a decrease in MWT is evident in all seasons but DJF. Again high model agreement in MWT$_{DIV}$~~generally projecting a decrease , and MWT $_{FF}$, MWT$_{FD}$, MWT$_{FDWS}$ and MWT$_{WS}$ suggesting an increase. MWT$_{FF}$ large slopes of +0.126, +0.193 and +0.072 shift the tug of war between the indices and suggest an overall increase in MAM. In SON, despite MWT$_{FF}$ producing slopes of +0.23, +0.25 and +0.11%/year, MWT$_{DIV}$ negative tilts of -0.143,0.123 and -0.043%/year, combined with negative results from other indices, produces a median within Table~~. There is high confidence in the JJA and DJF projections with 8:1 (positive:negative) and 1:7 slopes over Asia (Table. 2~~of -0.055 %/year. Within DJF and JJA, most slopes project an increase and a decrease in MWT , respectively. Over the 101-year period, DJF over Asia is projected to increase on average by +7 %, and at maximum by +30.9 %(MWT$_{FF}$, HadGEM3-GC3.1-HM~~). ~~Interestingly, only 50% of DJF and JJA lines within figure 7, have significant trends. A larger percentage is evident in MAM and SON.~~ Overall, an increase in MWT is projected for DJF over asia, and a decline is projected in JJA by 0.023%/yr and -0.014%/yr, respectively.

3.2.6 Australian Continent

A strong seasonal ~~gap~~ response arose in the slopes over the Australian continent ~~within figure~~ (fig. 8), with a clear decrease in MWT over DJF (1:10; positive:negative slopes) and MAM (~~summer and autumn~~1:8) and an evident increase for JJA (18:0) and SON (~~winter and spring) . The conditions of a)having all GCMs and b) all indices agreeing has been mostly met by this continent. JJA has all GCMs and indices producing significant trends, all projecting an increase. As displayed within Table 2, the average increase is of around +1.4 %with a maximum +4.4 % and minimum of +0.6 % over the 101 yearperiod. SON also had~~ 13:0) (Table.2). In fact, JJA has strong model and index agreement with all producing significant increasing trends with an average of 0.013%/year. SON too has a very similar agreement and trend but a lower number of significant slopes, at 72.22 % across ~~figure~~ fig 8. ~~In terms of amount of turbulence, compared to the other six continents,~~ For the remaining seasons, there is good model and index agreement on trend with just MWT$_{FF}$ EC-Earth-3P-HR projections projecting an increase in DJF and MAM MWT, with all the ~~y-axis is at its most negative on average, with a much smaller range. In terms of which season is on general most turbulent, in regards to MWT, JJA, SON and DJF are all at one point projected to have the largest amount of turbulence in at least one GCM and index~~rest suggesting a decline. The Australian continent does not have a high amount of projected MWT compared to the others, and is in fact at the greatest negative range (fig. 8 y-axes), so is the least turbulent continent.

3.2.7 Antarctic

There is a clear seasonality in the amount of MWT over the Antarctic, with ~~SH winter and summer~~ JJA and DJF being the most and least turbulent season. The large JJA (winter) values in ~~figure~~ fig. 9 place this continent second, after Asia, with the amount of projected MWT with the GCMs. Within this figure, only 6 projections suggest a ~~decline in MWT within this region. There are~~ decrease in MWT with 3 lines in JJA and 3 lines in SON across MWT$_{HTG}$ and MWT$_{FDWS}$ projections~~that show this decrease in MWT over the period~~. Despite this, there is quite strong model and index agreement, with all other indices, across all GCMs, projecting a significant increase in MWT. ~~DJF on average projected a rise of +32%compared to the amount in 1950. JJA, the most turbulent season, had an increase of +8.7%~~ The greatest increase is evident in DJF projections with a large rise of 0.31 %/yr or 31.3 % over the 101 year period. Few airlines travel over the Antarctic ~~,~~ but this result does put those few airlines at risk travelling, particularly in SH summer.

3.3 ~~Regional analysis~~

~~Section 3.1 highlighted sub-continental differences across the globe. Figure 10, 11~~

3.2.1 Continent summary

~~Line plots of relative percentage change over Africa for each year and individual season compared to a 1950 decadal global references, for each GCM; HadGEM3-GC3.1-HM, EC-Earth-3P-HR, and MPI-ESM1.2-XR and for each index. Line colour and marking differ for each season, with DJF blue and dashed, MAM green and dash dotted, JJA red and soild, SON purple and dotted. Annual change, which includes all seasons is black and solid.~~

Figures/MWT_figures/Africa.png

		North America	South America	Europe	Africa
Yearly	Slope Median	~~0.033~~ 0.052 +/- ~~0.019~~0.023	~~-0.015~~ -0.029 +/- ~~0.010~~0.036	~~0.039~~ -0.017 +/- ~~0.020~~ 0.077	~~-0.012~~ -0.013 +/- ~~0.005~~ 0.021
	~~Had~~ HM Median	0.063 +/- ~~0.018~~0.020	-0.042 +/- ~~0.010~~ 0.028	0.058 +/- ~~0.019~~ 0.066	-0.013 +/- ~~0.004~~ 0.024
	EC Median	0.050 +/- ~~0.018~~0.028	0.024 +/- ~~0.014~~ 0.039	-0.066 +/- ~~0.021~~ 0.087	-0.015 +/- ~~0.005~~ 0.018
	MPI Median	~~0.028~~ 0.046 +/- ~~0.021~~0.015	~~-0.014~~ -0.027 +/- ~~0.008~~ 0.016	~~0.045~~ -0.031 +/- ~~0.029~~ 0.021	~~-0.012~~ -0.009 +/- ~~0.006~~ 0.004
	Range	~~0.024~~ 0.016 +/- ~~0.015 -0.080~~ 0.023 to 0.094 +/- ~~0.009~~ 0.023	~~-0.110~~ -0.080 +/- ~~0.022 -0.064~~ 0.036 to 0.073 +/- ~~0.004~~ 0.036	~~to 0.094~~ -0.110 +/- ~~0.022 to 0.073~~ 0.077 to 0.114 +/- ~~0.021~~0.077	~~to 0.114~~ -0.064 +/- 0.021 to 0.017 +/- ~~0.007~~ 0.021
	Sig (%)	~~61.11~~ 66.7	~~88.89~~ 88.9	~~72.22~~ 66.7	~~55.56~~ 50.0
	no.pos, no.neg	12, 0	4, 12	~~,~~5, 7	1, 8
DJF	Slope Median	0.063 +/- ~~0.041~~ 0.031	-0.044 +/- ~~0.025~~0.045	0.043 +/- ~~0.041~~ 0.103	-0.032 +/- ~~0.009~~ 0.016
	~~Had~~ HM Median	0.063 +/- ~~0.036~~ 0.034	-0.093 +/- ~~0.025~~0.034	0.110 +/- ~~0.033~~ 0.096	-0.036 +/- ~~0.011~~ 0.018
	EC Median	~~0.073~~ 0.050 +/- ~~0.046~~ 0.025	~~-0.002~~ -0.003 +/- ~~0.024~~0.052	-0.091 +/- ~~0.057~~ 0.083	-0.032 +/- ~~0.010~~ 0.001
	MPI Median	NA	-0.037 +/- ~~0.021~~ 0.014	-0.064 +/- ~~0.024~~ 0.000	-0.008 +/- ~~0.004~~ 0.000
	Range	0.037 +/- ~~0.029 -0.122~~ 0.031 to 0.129 +/- ~~0.030~~ 0.031	~~-0.104~~ -0.122 +/- ~~0.032 -0.057~~ 0.045 to 0.045 +/- ~~0.007~~ 0.045	~~to 0.129~~ -0.104 +/- ~~0.043to 0.045~~ 0.103 to 0.155 +/- ~~0.019~~0.103	~~to 0.155~~ -0.057 +/- ~~0.041~~0.016 to -0.008 +/- ~~0.004~~ 0.016
	Sig (%)	~~33.33~~ 38.9	~~83.33~~83.3	~~50.00~~50.0	~~33.33~~ 33.3
	no.pos, no.neg	7, 0	2, 13	5, 4	0, 6
MAM	Slope Median	~~0.071~~ 0.069 +/- ~~0.047~~ 0.020	-0.033 +/- ~~0.020~~ 0.058	0.057 +/- ~~0.034~~ 0.090	0.010 +/- ~~0.007~~0.027
	~~Had~~ HM Median	NA	-0.034 +/- ~~0.018~~0.053	0.072 +/- ~~0.033~~0.070	0.024 +/- ~~0.015~~ 0.034
	EC Median	~~0.071~~ 0.069 +/- ~~0.047~~0.020	0.042 +/- ~~0.024~~0.048	-0.024 +/- ~~0.049~~ 0.086	0.010 +/- ~~0.007~~ 0.018
	MPI Median	NA	-0.060 +/- ~~0.032~~0.021	-0.050 +/- ~~0.023~~ 0.000	-0.009 +/- ~~0.004~~0.000
	Range	0.035 +/- ~~0.029 -0.099~~ 0.020 to 0.084 +/- ~~0.016~~ 0.020	~~-0.105~~ -0.099 +/- ~~0.049 -0.059~~ 0.058 to 0.083 +/- ~~0.007~~ 0.058	~~to 0.084~~ -0.105 +/- ~~0.047 to 0.083~~ 0.090 to 0.165 +/- ~~0.046~~0.090	~~to 0.165~~ -0.059 +/- ~~0.038~~0.027 to 0.033 +/- ~~0.019~~0.027
	Sig (%)	~~22.22~~ 22.2	~~55.56~~ 55.6	~~55.56~~ 55.6	~~55.56~~ 55.6
	no.pos, no.neg	4, 0	3, 7	6, 4	6, 4
JJA	Slope Median	~~0.069~~ 0.064 +/- ~~0.032~~0.025	-0.023 +/- ~~0.016~~ 0.057	-0.023 +/- ~~0.033~~ 0.071	-0.012 +/- ~~0.007~~ 0.021
	~~Had~~ HM Median	0.070 +/- 0.026	-0.002 +/- ~~0.014~~0.034	0.063 +/- ~~0.033~~ 0.044	-0.025 +/- ~~0.011~~ 0.017
	EC Median	~~0.057~~ 0.053 +/- ~~0.032~~0.017	~~-0.019~~ -0.017 +/- ~~0.018~~0.082	-0.040 +/- ~~0.037~~ 0.079	-0.008 +/- ~~0.007~~0.016
	MPI Median	0.077 +/- ~~0.047~~ 0.029	-0.037 +/- ~~0.017~~0.008	-0.032 +/- ~~0.021~~0.012	-0.009 +/- ~~0.006~~ 0.002
	Range	0.029 +/- ~~0.026 -0.046~~ 0.025 to 0.106 +/- ~~0.013~~0.025	~~-0.098~~ -0.046 +/- ~~0.039 0.052~~ 0.057 to 0.154 +/- ~~0.011~~ 0.057	~~to 0.106~~ -0.098 +/- ~~0.057~~ 0.071 to ~~0.154~~ 0.118 +/- ~~0.044~~ 0.071	~~to 0.118~~ -0.052 +/- ~~0.036t o~~ 0.021 to 0.024 +/- ~~0.016~~ 0.021
	Sig (%)	~~55.56~~ 55.6	~~55.56~~55.6	~~66.67~~66.7	~~55.56~~ 55.6
	no.pos, no.neg	10, 0	3, 7	5, 7	1, 9
SON	Slope Median	0.080 +/- ~~0.035~~0.056	-0.019 +/- ~~0.018~~ 0.046	-0.045 +/- ~~0.030~~ 0.096	-0.016 +/- ~~0.008~~ 0.028
	~~Had~~ HM Median	0.095 +/- ~~0.031~~0.042	-0.037 +/- ~~0.018~~0.030	-0.006 +/- ~~0.026~~0.104	-0.034 +/- ~~0.008~~ 0.034
	EC Median	~~0.013~~ 0.016 +/- ~~0.034~~0.070	0.036 +/- ~~0.024~~0.037	-0.078 +/- ~~0.034~~ 0.100	-0.015 +/- ~~0.009~~ 0.022
	MPI Median	0.085 +/- ~~0.051~~ 0.026	-0.028 +/- ~~0.010~~0.000	-0.045 +/- ~~0.023~~0.000	-0.014 +/- 0.007
	Range	-0.043 +/- ~~0.033 -0.079~~ 0.056 to 0.161 +/- ~~0.010~~0.056	~~-0.177~~ -0.079 +/- ~~0.030 -0.091~~ 0.046 to 0.090 +/- ~~0.008~~ 0.046	~~to 0.161~~ -0.177 +/- ~~0.042 to 0.090~~ 0.096 to 0.122 +/- ~~0.043~~0.096	~~to 0.122~~ -0.091 +/- ~~0.032~~0.028 to 0.028 +/- ~~0.012~~ 0.028
	Sig (%)	~~72.22~~ 72.2	~~55.56~~55.6	~~50.00~~50.0	~~55.56~~ 55.6
	no.pos, no.neg	11, 2	4, 6	3, 6	1, 9

Table 1. Seasonal and annual median slope values ~~from figure 3 to 6~~ across each GCM~~with HadGEM3-GC3.1-HM referenced as "Had"~~, ~~EC-Earth-3P-HR as "EC"~~ including ± standard deviation for medians and ~~MPI-ESM1.2-XR as "MPI"~~ranges.~~"Range" displays the spread across all significant slopes over GCMs. "Sig" displays the percentage of slopes for each season with significant slopes. "no. pos, no. neg" values indicating the number of significant positive or negative slopes.~~

Figure 6. Line plots of relative percentage change over Africa for each year and individual season compared to a 1950 decadal global references, for each GCM; HadGEM3-GC3.1-HM, EC-Earth-3P-HR, and MPI-ESM1.2-XR and for each index. Line colour and marking differ for each season, with DJF blue and dashed, MAM green and dash dotted, JJA red and soild, SON purple and dotted. Annual change, which includes all seasons is black and solid.

An overview of the slope distribution is highlighted in fig.10. As you can see the greatest increase in MWT is projected over the Antarctic by 0.52 %/yr or 52.52% over the 101-year period. The average is considerably lower at 0.14%/yr. The average seasonal trend for each continent and the number significant positive trends vs negative slopes are listed below and above the box-plots. For the Antarctic, all seasonal averages project an increase in MWT, with a ratio of 82 to 6, positive to negative slopes found in Fig 10. The second highest slope is the maximum trend over Asia at 0.31%/yr, although on average, there is a decrease by -0.005%/yr. This is due to the different seasonal trends, with a decrease in JJA and SON and a rise in DJF and MAM. North and South America and Europe have a similar maximum slope of 0.16, 0.15 and ~~12 focus on twenty-eight new smaller~~ 0.17 %/yr respectively. Over the three interestingly, the largest decrease in MWT is evident in Europe at -0.18 %/yr and then in South America at -0.12%/yr. With North America minimum (-0.04%/yr) in the same range as Africa (-0.09 %/yr) and Australia (-0.052%/yr). The projected average changes in MWT for North America, South America, Europe, Africa

Figures/MWT_figures/Asia.png

Line plots of relative percentage change over the Asian continent for each year and season compared to a 1950 decadal global references, for each GCM; HadGEM3-GC3.1-HM, EC-Earth-3P-HR, and MPI-ESM1.2-XR and for each individual index. Line colour and marking differ for each season, with DJF blue and dashed, MAM green and dash dotted, JJA red and soild, SON purple and dotted. Annual change, which includes all seasons is black and solid.

Figure 7. Line plots of relative percentage change over the Asian continent for each year and season compared to a 1950 decadal global references, for each GCM; HadGEM3-GC3.1-HM, EC-Earth-3P-HR, and MPI-ESM1.2-XR and for each individual index. Line colour and marking differ for each season, with DJF blue and dashed, MAM green and dash dotted, JJA red and soild, SON purple and dotted. Annual change, which includes all seasons is black and solid.

		Asia	Australia	Antarctic
Yearly	Slope Median	~~0.024~~ -0.007 +/- ~~0.016~~ 0.014	~~0.007~~ 0.003 +/- 0.004	~~0.129~~ 0.141 +/- ~~0.019~~ 0.021
	~~Had~~ HM Median	0.022 +/- 0.014	~~0.009~~ 0.004 +/- ~~0.005~~ 0.004	0.223 +/- 0.019
	EC Median	~~-0.020~~ -0.015 +/- ~~0.016~~ 0.018	~~0.016~~ 0.004 +/- ~~0.006~~0.005	0.129 +/- 0.021
	MPI Median	~~0.025~~ -0.007 +/- ~~0.016~~ 0.008	~~-0.002~~ 0.003 +/- ~~0.002~~ 0.003	~~0.084~~ 0.108 +/- ~~0.019~~ 0.025
	Range	~~-0.071~~ -0.080 +/- ~~0.009 -0.018~~ 0.007 to 0.240 +/- ~~0.004~~ 0.035	~~0.046~~ -0.022 +/- ~~0.014 to 0.206~~ 0.002 to 0.024 +/- ~~0.035~~ 0.008	~~to 0.020~~ 0.043 +/- ~~0.005 to 0.378~~ 0.014 to 0.402 +/- ~~0.025~~ 0.048
	Sig (%)	~~77.78~~72.22	~~55.56~~ 50.00	100.00
	no.pos, no. neg	~~,~~6, 7	7, 2	18, 0
DJF	Slope Median	~~0.070~~ 0.023 +/- ~~0.029~~ 0.026	~~-0.018~~ -0.012 +/- ~~0.008~~ 0.007	~~0.317~~ 0.310 +/- 0.051
	~~Had~~ HM Median	~~0.065~~ 0.050 +/- 0.025	-0.019 +/- 0.007	0.417 +/- 0.050
	EC Median	~~0.070~~ 0.055 +/- ~~0.032~~ 0.036	~~-0.018~~ -0.012 +/- 0.009	~~0.289~~ 0.274 +/- 0.046
	MPI Median	~~0.103~~ 0.003 +/- ~~0.064~~ 0.015	~~-0.015~~ -0.005 +/- 0.006	0.198 +/- 0.066
	Range	~~-0.062~~ -0.087 +/- ~~0.025 -0.053~~ 0.011 to 0.369 +/- ~~0.007~~ 0.071	~~0.152~~ -0.059 +/- ~~0.050 to 0.309~~ 0.004 to 0.023 +/- ~~0.060~~ 0.015	~~to 0.013~~ 0.101 +/- ~~0.009 0.523~~ 0.035 to 0.576 +/- ~~0.053~~ 0.118
	Sig (%)	50.00	~~66.67~~ 61.11	100.00
	no.pos, no. neg	8, 1	1, 10	18, 0
MAM	Slope Median	~~0.036~~ -0.004 +/- ~~0.027~~ 0.024	~~-0.009~~ -0.006 +/- ~~0.008~~0.007	~~0.149~~ 0.146 +/- 0.032
	~~Had~~ HM Median	0.043 +/- 0.024	~~-0.012~~ -0.008 +/- 0.008	0.231 +/- 0.031
	EC Median	~~-0.034~~ -0.021 +/- ~~0.032~~ 0.034	~~-0.012~~ -0.007 +/- ~~0.00~~ 0.008	~~0.123~~ 0.117 +/- 0.032
	MPI Median	~~0.026~~ -0.004 +/- ~~0.031~~ 0.013	~~-0.007~~ -0.001 +/- 0.005	0.104 +/- 0.032
	Range	~~-0.063~~ -0.095 +/- ~~0.032 -0.028~~ 0.013 to 0.245 +/- ~~0.008~~ 0.053	~~0.079~~ -0.036 +/- ~~0.026 to 0.192~~ 0.004 to 0.029 +/- ~~0.053~~ 0.012	~~to 0.020~~ 0.045 +/- ~~0.009 to 0.413~~ 0.020 to 0.457 +/- ~~0.044~~ 0.067
	Sig (%)	72.22	50.00	100.00
	no.pos, no. neg	7, 6	1, 8	18, 0
JJA	Slope Median	~~-0.042~~ -0.014 +/- ~~0.016~~ 0.027	~~0.014~~ 0.013 +/- 0.008	~~0.087~~ 0.077 +/- ~~0.026~~ 0.025
	~~Had~~ HM Median	~~-0.061~~ -0.000 +/- ~~0.028~~ 0.029	0.016 +/- 0.008	0.112 +/- 0.022
	EC Median	~~-0.042~~ -0.014 +/- ~~0.041~~ 0.036	~~0.022~~ 0.021 +/- 0.010	~~0.071~~ 0.067 +/- ~~0.025~~ 0.023
	MPI Median	~~-0.030~~ -0.024 +/- ~~0.014~~ 0.017	0.009 +/- 0.006	~~0.047~~ 0.046 +/- 0.027
	Range	~~-0.079~~ -0.121 +/- ~~0.041 0.006~~ 0.011 to 0.152 +/- ~~0.005~~ 0.052	~~-0.064~~ 0.000 +/- ~~0.023 to 0.100~~ 0.004 to 0.051 +/- ~~0.052~~ 0.012	~~to 0.044~~ -0.079 +/- ~~0.008 to 0.217~~ 0.017 to 0.251 +/- ~~0.034~~ 0.059
	Sig (%)	~~50.00~~ 44.44	100.00	94.44
	no.pos, no. neg	1, 7	18, 0	14, 3
SON	Slope Median	~~-0.055~~ -0.011 +/- ~~0.029~~ 0.024	~~0.013~~ 0.009 +/- 0.008	~~0.104~~ 0.088 +/- ~~0.034~~ 0.033
	~~Had~~ HM Median	~~0.023~~ 0.009 +/- ~~0.023~~ 0.024	0.014 +/- 0.008	0.168 +/- 0.026
	EC Median	~~-0.074~~ -0.070 +/- ~~0.042~~ 0.037	~~0.014~~ 0.011 +/- 0.009	~~0.087~~ 0.083 +/- ~~0.039~~ 0.034
	MPI Median	~~0.032~~ -0.010 +/- ~~0.036~~ 0.016	~~0.007~~ 0.006 +/- 0.005	~~0.084~~ 0.080 +/- ~~0.039~~ 0.036
	Range	~~-0.143~~ -0.159 +/- ~~0.016 0.0049~~ 0.015 to 0.302 +/- ~~0.0046~~ 0.057	~~-0.074~~ -0.007 +/- ~~0.040 to 0.250~~ 0.004 to 0.048 +/- ~~0.052~~ 0.015	~~to 0.036~~ -0.102 +/- ~~0.012to 0.349~~ 0.021 to 0.395 +/- ~~0.046~~ 0.074
	Sig (%)	66.67	72.22	94.44
	no.pos, no. neg	5, 7	13, 0	14, 3

Table 2. Seasonal and annual median slope values ~~from figure 7 to 9~~ across each GCM~~with HadGEM3-GC3.1-HM referenced as "Had"~~, ~~EC-Earth-3P-HR as "EC"~~ including ± standard deviation for medians and ~~MPI-ESM1.2-XR as "MPI". The same rows as Table 2~~ranges for Asia, ~~but with three final continents~~Australia, and Antarctic.

~~Line plots of relative percentage change over the Australian continent for each year and season compared to a 1950 decadal global references, for each GCM; HadGEM3-GC3.1-HM, EC-Earth-3P-HR, and MPI-ESM1.2-XR and for each individual index. Line colour and marking differ for each season, with DJF blue and dashed, MAM green and dash dotted, JJA red and solid, SON purple and dotted. Annual change, which includes all seasons is black and solid.~~

Figures/MWT_figures/Auz.png

Figure 8. Line plots of relative percentage change over the Australian continent for each year and season compared to a 1950 decadal global references, for each GCM; HadGEM3-GC3.1-HM, EC-Earth-3P-HR, and MPI-ESM1.2-XR and for each individual index. Line colour and marking differ for each season, with DJF blue and dashed, MAM green and dash dotted, JJA red and solid, SON purple and dotted. Annual change, which includes all seasons is black and solid.

and Australia are 0.032 %/yr, -0.019 %/yr, 0.004%.yr, -0.006%/yr and 0.004%/yr, respectively. These average shifts only equate to 0.4 to 3% over the 101-year period due to the large biases in averaging over such a wider area. To determine regional differences, our next section breaks down into sub-continental ~~areas of interest. Within these figures, results come from an average across indices with a significant trend . In some cases all six indices within the GCM are projecting insignificant trends so the model is not considered or plotted. This is noticeable by the lack of scatter from some GCMs in figure 10 side plots and grey shaded blocks within figure~~ zones.

3.3 Multi-model mean MWT regional analysis

The projected MWT trends across 28 sub-continental regions are highlighted in fig. 11. ~~Similar to figure 2g, the spatial map in figure 10 is the 1950-59 to 2040-49 decade percentage difference averaged over the three finest GCMs, regridded on to~~ This figure shows the difference between 1950-60 and 2040-50, as done in fig. 2, averaged over the GCMs and indices. The maximum, mean and minimum % of MWT over the ~~EC-Earth domain. However, if an index is not included in the scatter plots (insignificant) it has therefore been removed from each sub region in the spatial map, which averages across all GCMs and indices.However, when processing these figures, one should take care to note the spatial map in figure 10, which shows the decadal difference averaged across all seasons. If you break down the percentage change scatter in to each season (figure 11), differences in seasonal trends arise. Figure 11 breaks down the seasonal change for each region, averaged across the six MWT diagnostics.~~

~~The trends over a~~ 101 year period~~are discussed below. Further analysis was done, focusing on a future 30 year period (2020-2050) but is not included within this section due to large decadal variability within findings. Interestingly in some cases significance shifted, with some trends previously showing a trend no longer applicable and vice versa. This shows that having an 101 year period more effectively encapsulates the MWT trends in time, with~~ , relative to the 1950s decade (same as section 3.2) for each region is also displayed within this figure. The linear fit slope over each region can be found in fig.12.

The Antarctic, as clearly shown in fig. 11 and fig. 12, is a region of the globe with a ~~30 year periods linked to decadal variability.~~ relatively significant increase in MWT, at most by 0.3 %/yr in DJF. This increase is evident in all models but particularly in HadGEM3-GC3.1. The average amount of projected MWT over the Antarctic, across the indices, is just greater than the Alps (EUR2) and around a similar range as found in SA1 over the north Andes. This is highlighted within fig. 11, with the max, mean and min percentage of MWT over the period. These boxes help to infer the projected most turbulent regions, compared to our global threshold. The regions with the greatest

~~Line plots of relative percentage change over the Antarctic for each year and season compared to a 1950 decadal global references, for each GCM; HadGEM3-GC3.1-HM, EC-Earth-3P-HR, and MPI-ESM1.2-XR and for each individual index. Line colour and marking differ for each season, with DJF blue and dashed, MAM green and dash dotted, JJA red and soild, SON purple and dotted. Annual change, which includes all seasons is black and solid.~~

Figures/MWT_figures/Antartic.png

Figure 9. Line plots of relative percentage change over the Antarctic for each year and season compared to a 1950 decadal global references, for each GCM; HadGEM3-GC3.1-HM, EC-Earth-3P-HR, and MPI-ESM1.2-XR and for each individual index. Line colour and marking differ for each season, with DJF blue and dashed, MAM green and dash dotted, JJA red and soild, SON purple and dotted. Annual change, which includes all seasons is black and solid.

amount of turbulence are ASIA6 over the Himalayas, SA3 over the southern Andes, ASIA5 over Turkey and the middle east and then NA3 over the Rockies (fig. 11).

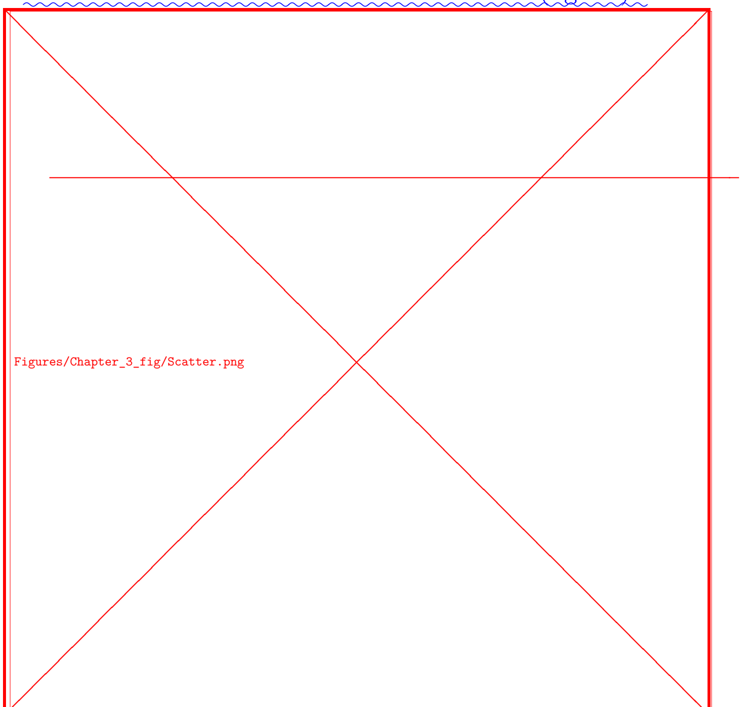

~~The spatial map displays the percentage difference between the 1950s and 2040s averaged across the three finer GCMs, similar to figure 5.2(g), but for each 28 regions. If indices are insignificant over a 101-year period, they are not included within area averaging. The line plots surrounding the map show the relative MWT percentage change from global threshold for each year, averaged over six MWT indices, for each new sub-region shown by a white box. HadGEM3-GC3.1-HM linear regression slopes and scatter are referred to as "Had", as previously done in Table 5.1 and 2, and coloured navy with a dash-dot line. MPI-ESM1.2-XR is referred to as "MPI" with a grey scatter and dashed linear regression line. EC-Earth-3P-HR is referred to as "EC" with black scatter and a solid line.~~

3.3.1 ~~North America; NA1-NA5~~

There are two notable regions in North America, NA1 and NA2, that project a large rise in MWT across all seasons (fig. 12). The North American continent is broken down into five regional areas. Region NA1 covers Greenland, Iceland and Canada north to ~~north east~~ north-east of the Hudson ~~bay~~Bay. Aircraft are known to travel through this

Figures/Overall_Contient.png

Figure 10. Distribution of all slopes within fig 3-9 legends for each continent, with the number of significant (95th confidence interval) slopes written above each violin plot, and the overall trend of slope (i.e. positive or negative) for each season written below each plot.

region, particularly over southern Greenland, when flying from Europe to North America and vice versa (Lane,2009; Doyle et al, 2005). MWT formation over Greenland is often associated with the passage of a surface cyclone, due to progression of easterly or south easterly wind flow over the ~~mountains~~ mountain's terrain, with 40 % of all significant turbulent events linked with this type of generation (Lane et al., 2009). ~~As discussed in Section 3.2, the percentage change is compared to a global average value of MOG MWT (dependent on index and model) and therefore percentage change on the y-axis of figure 10's scatter plots represents the amount of MWT in each region.~~ NA1 is the second most turbulent region in North America. Greenland is a known turbulent region of the globe, with every fourth day having at least one MOG turbulent PIREP ~~report~~ (Lane et al, 2009). In terms of seasonality, literature suggest MWT frequency is ~~similar to~~ like contiguous United States (CONUS), where some winter months (January) have had rates four times the amount of MOG MWT compared to spring months (May) (Lane et al,2009, Wolff and Sharman 2008).

~~Interestingly, NH summer HadGEM3-GC3.1-HM projections had the greatest average increase of +58.4 % over the 101 year period within NA1 (figure 11).~~ Once averaged over all GCMs ~~that's an increase of +30.5 %between~~ and indices (fig. 12), it's a projected increase of 18.2%, 16.2% 11.1 %, 7.4% for JJA, SON, MAM and DJF over the period (1950 to 2050~~for the summer season (JJA). NH autumn and spring project the same trend but at lower rates of +19.4 % and +18.0 %respectively. Interestingly, winter changes are more difficult to diagnose, with all indices projecting high inter-annual variability and insignificant trends , and therefore not included in figure 11 . Therefore, no definitive trends in MWT over NA1 in DJF . However, there are trends within surface winds speeds for NH winter between 1950 to 2050, evident in figure 12. Within this season, SON and MAM, an increase in median surface winds were projected, but weaker maximum wind speed. The evident increase in MWT frequency in SON and MAM could be linked to the average wind speeds, with increase evident in figure 12. However, the projected increase in MWT in JJA's, previously touched, within NA1 is not correlated to the surface wind speed changes, with a slight decline in median surface wind change for the HadGEM3-GC3.1-HM model. Only trends with significant slopes have been shown within figure 12, as done in the previous last two figures.~~).

~~Within figure 10, regions~~ NA2 ~~and NA4 are clearly projected to increase over the 101 year period. Here one can also note projected insignificant sloped lines in the side scatter plots. Despite all indices projecting a confident trend, their trends range in both the negative and positive spectrum. This has led to an overall average uncertainty within the scatter. EC-Earth-3P-HR's indices did not produce significant trends to be included initially in NA2 region, but within a break down of seasonality, its clearly linked to the model projecting a drop in MWT in NH summer and increase in NH autumn. NA4 projections too have a seasonal difference, with a general increase in all seasons but SON. Over all GCMs NH winter, summer, spring and autumn MWT rates are projected to shift by +21.6 % , -1.4% , +12.4 % and +17.9 % within NA2 over 101 years and by +7.2 % , +1.6 % -10.5 % and +10.9 % within NA4, respectively. In terms of relationships to surface wind speed, within NA2, DJF and JJA median surface wind speed projections corolate to the same positive or negative shift found in MWT results. This is not the case for SON and~~

_figures/LAT_Decadal_diff.png

~~MAM, with opposing trends. A similar outcome arose for NA4 in terms of the relationship between low-level wind speed shift and the change in seasonal MWT frequency.~~

covers central and western Canada and Alaska has a larger relative increase in MWT compared to the rest of the globe, with an average increase of 15.2 % (DJF), 14.1% (MAM), 13.1% (SON). Insignificant trends over the period for JJA. NA3 ~~encapsulates~~ covers part of the Rocky Mountain range ~~,~~ and is the projected most turbulent (mountain generated) region of North America ~~, with HadGEM3-GC3.1-HR data scattered at the 600% range.~~ (+648% at max, fig. 11). The Rocky Mountains are a ~~well documented~~ well-documented turbulent area (Wilms, Henrike 2020), with MWT the major source of turbulence over the western half of the USA (Wolff and Sharman,2008). ~~Figure 10 and 14 show a decline for~~ This papers limitations in terrain resolution means only parts of the Rocky Mountains are represented. In reality, the entire range will be turbulent. In contrast to the other North America regions, there is a projected decrease in the amount of MWT over NA3 ~~for all seasons but DJF(NH winter). EC-Earth-3P-HR DJF projections, averaged across significant indices, suggest an incredible slope of +1.64 % /year within this season. This steep slope is damped once averaged across GCMs, but overall they suggest an increase of 60.6%over the 101 years. NH summer, autumn and spring project a decrease of -58.3%,-30.9%and -41.2 % over the period within NA3. Interestingly, the median surface wind speeds in these seasons all project a decline. There is no evident trend within DJF surface winds (figure 12). This suggests a more turbulent future for the Rocky Mountain range within its current most turbulent season, but also a drop in the remaining three. Spring over this region, from climatology (Wolff and Sharman, 2008), can often have a peak in MWT similar to that in DJF~~ with DJF, MAM, JJA and SON -8.1 % -50.5%, -28.3%,-32.3%. ~~These results project a possible drop in this occurrence.~~ This significant decline MAM is the greatest decrease globally of all our projected trends.

~~The last regionin North America is NA5, which covers the southern states of the USA and the Caribbean. Within figure 1, it is evident that these southern USA states have pockets of MWT. However, once broken down into significant trends, these regions disappear. NA5 trends are therefore links purely to MWT over Haiti and the Dominican Republic. NA5 MWT rates were shown to decrease over the 101 years. These trends arose only in JJA, SON and MAM (figure 11) by -1.26 %, -0.59 %and -1.73 % over the entire period . This decrease is also linked to drops in median and maximum surface wind flow, but only for SON and MAM. JJA has a mix across two significant trends for median surface wind flow.~~

~~Seasonal trends for MWT over 28 sub-continental regions, highlighted in figure 10. Over the 101 year period, shaded grey if no significant trend. The figure breaks down results into columns associated with the three GCMs, as evident by labelling on the x-axis. DJF, JJA, MAM and SON displayed in subplot 'a','b','c' and 'd'.~~

3.3.1 ~~South America; SA1-SA3~~

The 2^{nd} greatest global decrease is found in South America in SA2 in DJF by -46.5%. Within this region, all other seasons follow this trend decreasing by -17.2%, -24.2%, -36.4% in MAM, JJA and SON. There are three regions in South America shown in ~~figure 10~~Fig 11, that break down the Andes mountain range into northern (SA1), central

(SA2) and southern (SA3) ~~regions. Central and Southern Andes are projected to~~ sections. Findings suggest the southern parts of the Andes in SH winter (JJA) could become considerably more turbulent~~, with amounts equal to and just greater than NA3. Northern and Central Andes projected MWT amounts are projected to decline within most GCMs for~~ . Fig. 11 shows the difference between 2050 and 1950, and highlights an evident MWT increase for SA3 for all seasons. ~~The one outlier model and season in SA2 is EC-Earth-3P-HR's SON, which projects an increase within SH spring (figure 11.d) of +0.15 %/year. HadGEM3-GC3.1 projected decline is greater, and so on average projects a decline within DJF , JJA , MAM and SON by -11.6 %, -42.9 %, -25.8 %, -20.3 % and -11.6 % , respectively for SA2. There's high confidence that MWT will reduce, across all seasons ,~~ However, this is decadal variability, as the trend over the century only projects JJA to increase in MWT by 9.5%. Such an increase may seem relatively small, compared to other slopes, but it is already the second most turbulent region of the study (mean of 670.4%, fig. 11). The remaining seasons in SA3, and all within SA1 ~~, with strong significant model agreement~~and SA2 project a decrease in the amount of MWT.

The ~~Northern Andes MWT reduction is greatest in DJF by -22.3 %, then in MAM -16.0% , next SON -9.1% and finally JJA at -8.8% over 101 period. Interestingly, EC-Earth-3P-HR projected weaker surface median wind speed, across all seasons (if applicable). However, stronger surface maximum and median winds are evident in remaining GCMs. SA2's connection to surface wind speed is more apparent. SON's increase in EC-Earth-3P-HR could be linked to the slight stronger median surface winds. The decline in HadGEM3-GC3.1-HM, within this season, is possibly linked to stronger maximum wind speeds, but not median winds. Very similar results obtained for DJF. MAM has only one model with significant surface wind speed, it is in fact decreasing. However, surface winds in JJA are increasing, an opposite trend to how MWT is projected to shift in this area and season. This season has only one wind trend for comparison, but could suggest a seasonal dependence of MWT on low level wind speeds in~~ 3^{rd} greatest global decrease in MWT is within Asia in ASIA6, with a drop of -36.4 % over the century in JJA. Over Asia, eight zones were chosen for further analysis with ASIA6 encompassing Indian and Sri Lanka. Note that some regions have parts of Europe and the Australian continent within them. The remaining seasons too project a drop in MWT for AISA6 but by considerably lower amounts with -5.7% in DJF, -9.6% in MAM and -14.1% in SON. The largest amount of projected MWT is found in Asia in zone ASIA4. This area includes the Himalayan mountain range and Tibetan plateau within it. There are disagreeing trends across the model projections for this region.

~~There is variation in the GCM projections for the Southern Andes (SA3). Figure 10 projects a rise in MWT overall between the two decades, but only one GCM projects this rise (EC-Earth-3P-HR)and due to a wide range of index outcomes, has an insignificant slope. The remaining two GCMs project the opposite scenario with a decline in MWT frequency. These trends continue into the seasonal breakdown in figure 11 with HadGEM3-GC.1~~ One should take a moment to notice that despite a decrease in decadal difference between 1950 and ~~MPI-ESM1.2 project a drop in MWT across all seasons. A tug of war between an increase and decrease for each season arises with SON and MAM decreasing overall by -11/~~2050 (fig. 11), a trend over the period is increasing by a small amount of 2%~~and -2.3% but~~

Figures/MWT_figures/Seasonal_Slop_END.png

Figure 12. For each of our 28 regions, the linear regression slope between 1950 to 2050 for each season is displayed, with an average taken over the three high resolution GCMs; HadGEM-GC3.1, MPI-ESM1.2-XR and EC-Earth3P-HR. The area in which each region represents is found on fig. 11.

~~DJF and JJA projections dominated by the single GCM (EC-Earth-3P-HR) with an average of +17.7% and +2.8% across all GCMs.~~

~~Over North and South America, a trend has arisen with EC-Earth-3P-HR projections differing to MPI-ESM1.2-XR and HadGEM3-GC3.1-HM, usually with an opposing warming trend. This model variation is also evident within other continents. Within figure 12~~, ~~SA3 has one significant trend, with a drop in median surface wind speeds with MAM HadGEM3-GC3.1-HM. This season and model projects a drop in MWT, suggesting a possible decline linked to low-level wind speed.~~ 2.4% 1.4% and 1.6% in DJF, MAM, JJA and SON. This is due to EC-Earth-3P-XR projecting a significant increase and monopolising the average trend, despite two out of the three projecting a decrease.

3.3.1 ~~Europe; EUR1-EUR3~~

~~There are three regions over Europe analysed in figure 10. It should be noted that EUR3 includes some areas in Africa and Asia. Similar to NA5, EUR3 had more patches of MWT in figure 1.g than figure 10, that have disappeared when considering the trends in time. figure 10 only shows the confident trends in MWT, rather than the existence of MWT. Figure 11 encapsulates differences across the seasons within this region. There's strong model agreement on a projected decrease in the amount of MWT by -8.1% in JJA within EUR3. HadGEM3-GC3.1-HM~~ ASIA5 and ~~MPI-ESM1.2-XR projections show a decline in both median and maximum surface wind speed. A decline in low-level wind speed, in both the median and max, are evident~~ ASIA3 are the 2^{nd} and 3^{rd} most turbulent regions in the Asia. ASIA5, which covers Azerbaijan, Georgia, Turkey and parts of Iran, Kazakhstan and Turkmenistan, has a relatively large increase in MWT over DJF with a 25.3% projected rise from 1950 to 2050. Despite this rise, a decline is projected for the remaining seasons ~~. In terms of MWT, SON overall decreased in frequency by -2.2% over the 101 period, despite a warming trend in EC-Earth-3P-HR projections. DJF and MAMare projected to increase on average by +13.9% and +4.4% over the century within EUR3.~~

~~In contrast, EUR1 and EUR2 have all seasons, in most GCMs, projecting an agreed upon~~ by 1.4'% in MAM, -1.5% in JJA and -23.3% in SON. Clear seasonal dependence on the trend in time ~~. Despite, MPI-ESM1.2 projecting a slight drop in MWT in EUR1 summer rates, this season had an overall increase in MWT by +2.7% . Larger increase found in SON and MAM, with a percentage change of +5.1% and +4.4%. JJA and MAM MWT rise are consistent with stronger median surface winds (figure 12). DJF had no significant trends in time, so is shaded in grey within figure 11.a . EUR2 has all seasons projecting a decrease in MWT. There is quite strong confidence for a decline~~ for this region. In contrast ASIA3, projects an increase in ~~DJF, with all three GCMs projecting~~ all seasons by around 1-2% over the period.

AFR5 in Africa has joint 6^{th} greatest decline (joint with NA3 in JJA) with a drop of ~~-14.7% on average over the period. SON, JJA and MAM follow suit dropping by -18.3% , -13.1% and -6.5%. Interestingly, DJF and MAM have only one model each projecting a trend in figure 12. A decline in median surface wind speed is evident. EUR2, which encapsulated the Alps mountain range, is the most turbulent projected region of Europe. This projected decrease in such a turbulent region, will aid future flights through this busy continent.~~

~~Trends in surface wind speed for each sub-region shown in figure 10. The Maximum and Median winds are discussed individually with notation 'Max' and 'Median' for all GCMs. Each model is donated similar to that in Table 1 & 2 with HadGEM3-GC3.1-HM referenced as 'Had', EC-Earth-3P-HR as 'EC' and MPI-ESM1.2-XR as 'MPI'. DJF, JJA, MAM and SON displayed in subplot 'a','b','c' and 'd'. The grey zones depict insignificant GCM projections.~~

3.3.1 ~~Africa; AFR1-AFR6~~

-28.3% in DJF. Africa is split into six regions, with AFR1 slightly cutting off the bottom of Spain and Italy but primarily covering Morocco, Algeria, Tunisia and Libya. AFR1 is technically projected most turbulent region in Africa, bur AFR3 is a close second. AFR3 includes regions in the Middle East (Asia). ~~AFR1 and AFR3 display a clear decline in MWT over our projected period of interest within figure 10. There are seasonal and model disagreements, evident in figure 11. Within AFR1, models agree on a decline with DJF, SON and mostly within MAM projections, with two out of three projecting a decline. Within JJA, EC-Earth-3P-HR projects a moderate increase (relative to the decrease projected by MPI-ESM1.2-XR) resulting in an overall average increase in +16.3 % over the 101 years. DJF, SON and MAM too project a moderate percentage change of -26.1% ,-15.2% and -17.6%. Median surface wind were found to weaken within these seasons (figure 12). Results for AFR3 are very similar to those for AFR1, but with an increase found in DJF. EC-Earth-3P-HR projects a steep slope of +0.75%/year. However, HadGEM3-GC3.1 projects a smaller yet still moderate slope of -0.4%/year. On average, AFR3 increase in DJF by +15.9% and decrease in MWT within JJA, SON and MAM by -5.8% , -16.9% and -7.9% . Interestingly, a mix of trends arose for surface wind flow in JJA. The decreases in MAM and SON MWT results are consistent with the decrease seen in low-level median wind flow.~~

AFR2, AFR4, AFR5 and AFR6 have a much smaller amount of MWT compared to AFR1 and AFR3~~, this is shown by the negative values the scatter remains in with figure 10. In general a~~. A decrease in MWT ~~projected across these areas. However,~~ is projected in all regions in Africa, in all seasons on average. EC-Earth-3P-HR ~~project a notable increase in AFR2 and ARF6 within figure 11. This leads to an overall increase of +8.5% in MAM within AFR2 and +6.2% in JJA in AFR6. This summer increase is linked to stronger median surface winds in this model (figure 12). However, within AFR2, all surface wind speed changes are projected to get stronger in DJF yet MWT rates are dropping by -7.5%. Despite median surface wind trend often associated with the corresponding trend in MWT, there are a few exceptions with differing outcomes. JJA and SON project a slight decrease in MWT of -0. 5% and -1. 9%. AFR6 has a slight increase in SON by +1.1%, but declines in DJF and MAM by -9.2% and -4.9% over the 101 year period. The most considerable decrease in Africaare found within AFR5, with DJF MWT rates decreasing by -61.6% over the 101 year period. EC-Earth-3P-HR is the considerable driver in these large trends (figure 11.a). A decrease in MWT also evident in JJA, SON and MAM, with strong model agreement, but at lower rates of -6.8%, -2.20% and -6.6% for AFR5. The change in maximum wind speed decrease in all seasons within ARF5, correlating to the MWT trend. AFR4 has its most notable decrease in MWT within SON by -12.0 %, followed by MAM by -6.4% and then similar declines in MWT within DJF and JJA on averageacross the GCMs at -2.4% and -2.3%.~~

3.3.1 ~~Asia; ASIA1-ASIA8~~

~~Over Asia, eight zones were chosen for further analysis. This was done due to differing trends on initial analysis and MWT developing in many regionsover this continent. The largest amount of projected MWT is found in Asia in zone ASIA4. This area includes the Himalayan mountain range and Tibetan plateau within it. As figure 10 clearly shows, this area is decreasing in percentage of MWT by the end of the century compared to the beginning. However, figure~~ projects an increase in some regions, which wins the tug of war in trends for the decadal difference between 1950 and 2040 (fig. 11~~, shows this decline is only evident in SON, with two significant slopes in models EC-Earth-3P and MPI-ESM1.2-XR projecting a drop of -18.4% on average over the period. This is linked to weaker median surface winds this season, as evident in figure 12. Within ASIS4, both JJA and MAM have HadGEM3-GC3.1-HM and MPI-ESM1.2-XR modelsprojecting a decline in MWT, with EC-Earth-3P-HR projecting a considerable increase. In the tug of war, EC-Earth-3P monopolizes MAM projections due to its steep slope of +0.64 %/year. This leaves ASIA4 increase on average of +5.0% in MAM. The other two GCMs dominate the JJA averages, resulting in an overall decrease of -8.5% over 101 years. HadGEM3-GC3.1-HM, despite projecting a decrease in JJA, projected stronger maximum surface winds but weaker median surface wind flow. Interestingly, EC-Earth-3P-HR MAM median surface winds projected a rise over the 101-year period, a different trend to that examined above around MWT percentage shifts. Only HadGEM3-GC3.1 projects significant slopes in DJF, with a projected increase of 18.3%. One can note an almost equal shift in MWT across seasons from SON towards DJF. This level of increase within the most turbulent projected region of the globe is a noteworthy finding, considering that long-haul flights often travel through this area. The median surface wind flow projecting a decline over DJF within figure~~), but not the overall trend (slope) over the century (fig. 12~~, suggests this increase is possibly linked to upper-level dynamical variation. The strengthening in upper-level jet streams in time has lead to an increase in clear air turbulence production. As projected MWThas large seasonal shifts throughout the globe, perhaps alterations in the upper-level jet with climate change is also having a direct or in-direct impact on MWT production. Further research should be done on this possible connection.~~

~~ASIA5~~). Kim et. al (2023) which did a similar study but using more indices, and ~~ASIA3 are the 2nd and 3rd most turbulent regions~~ different models, found a decrease in ~~the Asia. ASIA3 interestingly, within figure 10, has two significant slopes both projecting different trends in time. These two opposing trends arise from averaging over a large region and seasonal variation. EC-Earth-3P-HR is not within this scatter plot but has significant trends when broken down seasonally, with a DJF trend of +2.0%/year. DJF, averaged over GCMs, has an increase of +112.3% in MOG MWTover this region. Fascinatingly, the remaining seasonal project an overall decrease in MOG MWT, by -36.1 % (MAM), -17.4% (JJA) and -16.6% (SON). A trend also evident this regions median and maximum surface winds (figure 12). No significant surface wind trends found for DJFin AISA3 or ASIS5. However~~summertime MWT agreeing with our trend. However, this paper also found a sharp rise in wintertime MWT, ~~there are significant MOG MWT within DJF in ASIA5, with an increase of +123.4%. SON also projected an overall average change of +23.0%.~~

A decrease was found in JJA and MAM by -5.9% and -7.9%. In relation to surface wind speeds trends , this region had JJA, MAM and SON all with projected declines in median and maximum. differing to our projections,

The remaining regions in Asia propagate below zero in figure 10 scatter plots, and therefore have considerable less MWT amounts than the three aforementioned ASIA zones. Within figure 11There are three regions of Europe included in this sub-continent analysis. Only EUR1 projects an increase in MWT, ASIA2 EC-Earth-3P-HR projects a decline in MWT over all seasons in this region, possibly associated with the slight drop over southern Japan (figure 10). The remaining two GCMs, if applicable, projected an increase in MWT in all seasons. This is further evident in figure 10 ASIA2 side plot, with MPI-ESM1.2 and HadGEM3-GC3.1 projecting an increase, but EC-Earth-3P-HR projecting a decline. Overall the maximum increase in this region arose in JJA at +2.4% in JJA and minimum in SON of +0.8% over the 101 years. ASIA1, has a slight increase across all GCMs (strong model agreement) and seasons, with the maximum percentage change over the century at +1.7% in SON and minimum of +1.4% in DJF.

The final three regions of Asia encompass Indian and Sri Lanka (ASIA6), south eastern Asia (ASIA7/8) and a few countries in the Australian continent (Papa New Guinea; ASIA8). ASIA6-8 have a general decline over the period, with a decrease in SON and MAM. Although a slight MAM increase in HadGEM3-GC3.1 with a shift of 2.5-5% across seasons excluding DJF. Interestingly, there are no significant trends in ASIA8. IN DJF, ASIA6 projects extremely small increase over the 101 years (-0.08%) , ASIA7 projects a light increase (1.86%), with ASIA8 finding a decline in MWT of -10.1% . Within the JJA projections, ASIA6 has a relatively moderate decline of -9.9% , ASIA7 projects slight increase of +0.5% and ASIA8 has two disagreeing GCMs projecting a slight increase (HadGEM3-GC3.1-HM) and decrease (EC-Earth-3P) overall resulting in a small increase of +0.76% over the centurytime over winter across Europe. Please note that there are some European countries included in the Asia overlap, due to wide boxes. EUR1 covers the Scandinavian counties, with this increase arising around the Scandinavian Peninsula (Scandes) and over Svalbard. Another region of interest is EUR2 which covers the Alps, the Pyrenees and Apennines mountain ranges. Results are only significant in SON, due to large variability in indices and models. A significant decrease of -20% was projected in this climatology turbulent season.

3.3.1 Australia and Antarctic; AUZ1, AUZ2 and ANT

As discussed there There are technically three regions within the Australian continents, with ASIA8 covering both Asia and the Australian continent. AUZ1 and AUZ2 are located south of ASI8 over Australia and New Zealand. AUZ1, which includes areas in the Australian country like New South Wales, Victoria and Tasmania , had more features within figure 1, but only a few scattered patches within figure 10's global map. The lines within AUZ1's scatter plot both project an overall has a slight decrease over the 101 years. Within figure 11, the white patches occur often in subplots a,b,c and d within the AUZ1 section. They suggest an extremely small, almost no change result. However, in MAM and JJA, there are slight shifts within HadGEM3-GC3.1 and EC-Earth-3P results with a decrease of -3.8% in MAM and increase of +1.6% in JJA over the 101 year projected period. These trends correlate to shifts in low-level surface wind speed shifts within the period. period by -1 to -4 % over all seasons. There are

Figures/MWT_figures/Wind_Speed_slopes.png

Figure 13. The average and maximum low-level wind speed trends within each region. Highlighted in red and blue if change in wind speed is the same as shift in MWT within the same area.

greater season differences in AUZ2, which covers New Zealand, looks to be increasing in time within figure 10 . SH winter and spring (JJA, SON) have full model agreed projected positively sloped trends in time, increasing by +8.4% and +5.9% over the period. However, DJF(SH summer) and MAM (SH autumn) are decreasing in time, with GCMs agreement, by -9.4% and -8.1% . An increase of 4.3% in JJA but a decline by -10% in DJF, -2.3% in MAM, -1% in SON. Interestingly, the amount of MWT in this box is greater than many regions in Asia and Africa.

There are no new regions in the Antarctic, with similar projections evident across continent. However, the scatter box, titled 'ANT' do show the average over the previous line plots in figure 9 . The average amount of MWT over the Antarctic, across the indices, is just greater than the Alps (EUR2) and around a similar range as found in AFR1 over the Atlas Mountains. The increases here correlate to the findings in Table 2, with an steep increase found in DJF, particularly in HadGEM3-GC3.1 model. This shift may partly be associated with increased low-level and upper-level wind speed over this polar regionAs is highlighted clearly on fig. 12, there are more places in the globe projecting a drop in the MWT than increase. Kim et. al (2023) projected an increase in MWT in the mid to high latitudes and a decline usually in the Tropics. This is somewhat the case within our projections, although South America and the Rockies project a decline in line with the tropical regions. Kim et. al (2023) found that their changes in MWT were linked to low-level wind change. Fig. 13 shows if any regions have a similar confident trend in time for both MWT projections and mean or maximum 10m wind speed variation in time. The Antarctic trends in DJF and JJA are linked to an increase in the average and maximum low-level winds. The British Antarctic Survey found surface winds strengthen by 15% since 1980. This is a trend evident in figure A.1 to 5 and within figure 12, with all GCMs and both median and maximum surface wind trends projecting stronger flow for the Antarctic continent. The mean JJA winds and maximum SON winds over NA2 are increasing over the period, this agrees with our change over Canada and Alaska. Over North America, the decrease in MWT over the Rockies in SON is linked to a decrease in the maximum wind speeds. The decrease over India and Sri Lanka is also associated with the decrease but in the average low-level wind. The choice to include the average and maximum wind speed was done to encapsulate if the wind speed on average was increasing, rather than just if the number of maximum wind speeds increased.

Through the use of

4 Conclusions

Using three HighRes-MIP CMIP6 GCMs, this study investigates the modeled investigated the modelled projections of global MWT turbulence over a 101-year period. Through an initial comparison between the 1950-60 and 2040-50 decade, one we found coarser models were not able to could not detect as much detail as their finer counterparts. This was linked to improved gradient and terrain height information. This study continued only with three higher resolution models; HadGEM3-GC3.1-HM (25km), EC-Earth-3P-HR(36km) and MPI-ESM1.2-XR (34km). Each MWT index was broken down and analysed initially through continental yearly analysis (figure fig 3 to 9). Regional dependencies arose around model and index agreement, with seasonal components an important contributor to results. Finally, a sub-regional approach was discussed, where seasonal MWT and surface wind speed trends were analysed.

On average, the North American continent had an increase in MWT~~since the starting decade~~. However, a lot of the trends in time were not ~~deemed~~ significant. On further sub-continental analysis, the zone encapsulating the Rocky Mountain range ~~,~~ was shown to be decreasing in the amount of MWT in all seasons~~but NH winter. Within DJF, increase of +60.6% in MOG MWT arose, with similar yet opposite rates of -58.3%, -41.2 % and -30.9% for JJA, MAM and SON.~~ . Greenland, a region used often for transatlantic travel, ~~is increasing~~ had increased in the amount of MWT, with its greatest shift in JJA by +~~30.5~~18.2%. Over South America, a decrease in MWT was evident from initial analysis. ~~There is~~ This decline in MWT continued into further sub-continental analysis, with strong model agreement ~~that the North and Central~~ on northern and central regions of the Andes ~~will have a large decreases in MOG MWT within SH summer (DJF), with drops of -22.3% and -49.2%, retrospectively~~projecting a decline. Southern Andes ~~have a shift across seasons, with DJF and JJA projecting increases in MWT, at most in DJF at +17.7%. Although SON and MAM, project a decline , at most at -11.2% in SON.~~ projects an increase in SH winter by 9.5% but over remaining seasons a decrease was evident.

~~Over Europe and Africa, a decline in MWT is evident over~~ This decrease in projected MWT continued across Africa, with the greatest decline over the Madagascar in DJF by 28.3%. Strong agreement across all seasons for a decline in MWT over this continent. In comparison, Europe's projections suggested a decrease in just one region covering the Alps and ~~Atlas Mountain ranges . NH autumn over the Alps has the largest decline of -18.3%, followed quickly after by DJF at -14.7%. DJF had a decline of -26.1% over parts of the Atlas mountains, with a decline~~ other central European mountain ranges in MAM. MAM was the only season with a significant trend in time, this was due to a wide spread of index and model trends. However, a rise in MWT evident ~~across the entire African continent. However, large increases arose over Asia, with two regions projected an increase above +100% (ASIA3/5) in DJF. Interestingly, over the Tibetan plateau and Himalayas, MWT rates increased within DJF and MAM by +18.3% and +5.0%, but a similar yet opposite increase for SON and JJA of -18.4% and -8.5%. The last regionof significant change occurred over the Antarctica peninsular, with DJF and JJA increasing by +32% and +8.7%. Further regions were explored, with many areas having a close trend related to median surface wind speed and it change over the century~~in Scandinavia and the Arctic circle in Svalbard.

An increase in MWT was projected in one model over the Himalayan mountain range and Tibetan plateau (region; ASIA4) which lead to an on average increase in MWT. However, ~~several regions and seasons were less dependent on the low-level wind speeds. In terms of significance to forecasting operations in the aviation sector, results over Asia, Europe, North and South America are key, considering the high density of flights that travel over these regions.~~

~~Overall, a mixture of MWT changes arose across the globe. The aviation sector should be aware of the future projections in MWT, particularly for those were large increase over the 101 year period were evident, such as Asia, Greenland and the Antarctic. Future work should focus on differing warming scenarios, other to SSP5-8.5, to get a full picture of possible future MWToutcomes~~the remaining two projected a smaller relative decline. This is a limitation of the final summary results in our sub continental results, with averages over models and indices taken. As discussed in our continental review, there are often disagreements between GCMS and the methods to diagnose MWT.

4.1 Limitations

This paper acknowledges that modelled atmospheric and ocean data is used, all projections are based on a future scenario of the globe.SSP5-8.5 is the extreme climate warming scenario with no action, with little mitigation or adaptation (Deng 2022). ~~One~~ As discussed in methodology, one limitation within previous work (Sharman and Pearsons~~(~~, 2017~~),~~ ; Kim et al.~~(~~, 2023) ~~,~~ that continues within this paper is that MWT often occurs downstream from mountain ranges (Wilms, Henrike,20220). Our region should encapsulate source of the downstream MWT due to our inclusion of slope gradient, but may miss MWT which travels far distances due to certain meteorological conditions (Lane et ~~. al~~al., 2009). Our terrain is sourced from our models, and not a secondary source with higher ground resolution. Future studies could apply such resolutions to fully capture other regions of MWT.

Appendix A: Breakdown into Indices; Two decadal comparison

Figure A.1, A.2 and A.3 display the decade difference for HadGEM3-GC3.1-HM, EC-Earth-3P-HR and MPI-ESM1.2-XR individually, for each index, rather than averaged (~~figure~~ fig. 2). These figures also include the decade difference in daily maximum (g) and median (h) surface wind speeds. As mentioned in Section 2.0; Methodology and Data, low-level wind speed is a variable within our MWT indices. One area of investigation is to understand if a shift in MWT is linked to possible changes in surface winds. Deng et al. (2022), using different, coarser CMIP6 GCMs and observational data, found CMIP6 GCMs correctly reproduced the decreasing trends (between 1980-2010 and 2070-99) in near surface winds in North America, Europe and East Asia. They did on average simulate faster wind speeds at coastal areas than inland, and have shown seasonal variations. Please note these wind speed percentage change only displays results over regions in which MWT arises, other areas excluded for ease of comparison.

Within the HadGEM3-GC3.1-HM (25km) model, a general increase in maximum wind speed is apparent in ~~figure~~ fig. A.1.g, with a larger percentage change compared to the change in average surface wind speed (~~figure~~ fig. A.1.h). The maximum surface winds have relatively large percentage shifts over Greenland, the Antarctic and Asia. These regional increases correlate the rise in MWT frequency in many indices within this figure. Interestingly, average wind speed has more regions that project decrease over the continents, than maximum wind speed, particularly interesting is the decline on the coastlines of the Antarctic between 60-180 °E. One could argue the changes in wind speed, in both maximum and average, correlate to projected MWT percentage differences in such indices as MWT$_{FD}$, MWT$_{FDWS}$,MWT$_{WS}$. Within this figure, the projected outcomes from these indices are relative similar within the HadGEM3-GC3.1-HM model.

Interestingly, MWT$_{DIV}$ (~~figure~~ fig. A.1c) projects a very notable MWT decline across the globe, including southern Greenland, the North America Rocky, Central and Southern Andes and the Himalayas. A decline in maximum wind speeds arises over the Antarctic and north west Greenland, regions where MWT$_{DIV}$ projects a drop in MWT frequency between the two decades. MWT$_{HTG}$ (~~figure~~ fig. A.1a) is an index shown to effectively represent MWT over North America ~~, according to ROC curve analysis from~~ (Shaman and Pearson's~~(~~, 2017). This index projects either no change or a decline in MWT over southern Greenland, USA and Canada. Despite similarities to MWT$_{DIV}$, MWT$_{HTG}$ differs over the African and Asian contentment, with an increase in turbulence at the southern edge of the Tibetan Plateau. The most notable index within ~~figure~~ fig. A.1 is MWT$_{FF}$, with a pronounced decline projected over the northern Andes, eastern Africa, the Himalayas and Indonesia and a substantial increase projected in other regions of the globe. Except for similarities in North America, MWT$_{FF}$ and MWT$_{HTG}$ have almost opposite projections. A weakening in MWT$_{HTG}$ projections may be associated with polar amplification weakening the meridional temperature gradient.

The EC-Earth-3P-HR (36km) and MPI-ESM1.2-XR (34km) too have the most notable change found within MWT$_{FF}$. These two models project a greater overall increase over Asia than HadGEM3-GC3.1-HM within this index. There is a notable drop in the number of regions producing MWT within MPI-ESM1.2-XR projections. However, in comparison to the mid-range and coarser models, a large percentage of the globe is still incorporated. MWT$_{DIV}$ within ~~figure~~ fig. A.3 projects a similar decrease to that evident in HadGEM3-GC3.1-HM (~~figure~~ fig. A.1c) results, over the regions available. Interestingly, EC-Earth-3P-HR projects a decrease in some regions, using MWT$_{DIV}$, but a much smaller percentage change. In some cases MWT$_{DIV}$ project a slight increase in areas which decreased in ~~figure~~ fig. A.1 (North/South America). Despite these difference, these spatial maps from ~~figure~~ fig. A.1 to 5 suggest a greater variation in trends in the indices than GCMs.

The change in surface wind speed marginally differs across the GCMs. Although, EC-Earth-3P-HR compared to HadGEM3-GC3.1-HM projects weaker winds inland over Asia, Greenland and North America, for change in average wind speeds. MPI-ESM1.2-XR also projects weaker winds over Asia within ~~figure~~ fig. A.3 (h). These differences highlight the impact of the average surface wind on MWT$_{FD}$, MWT$_{FDWS}$, MWT$_{WS}$ projections. These weaker winds link to negative changes in MWT, particularly over Asia.

Appendix B: Clear air turbulence indices

These are the indices used in combination with our terrain height, gradient and wind speed requirements to calculate mountain wave turbulence. As mentioned in methodology we focus on 200 hPa, note some indices use a vertical component and spread from 250 hPa to 150 hPa. These indices are combined with Ds to create MWT indicies (Section 2.1). Please contact the corresponding author for the MOG thresholds for each MWT index and ensemble model. Please note that these thresholds should be applied to the same HighResMIP GCMs used within this study.

Figures/MWT_figures/HadGEM.png

Figure A1. The decade percentage difference in MWT between 1950-59 and 2040-49, for the six MWT indices using the Met. Office Model HadGEM3-GC3.1-HM with grid spacing domain of 25km, averaged over three ensemble member runs (a-f). The change in maximum and median wind speed, between these two previous mentioned decades, within HadGEM3-GC3.1-HM is highlighted in subplots g and h respectively.

Figures/MWT_figures/EC_Earth.png

Figure A2. The decade percentage difference in MWT between 11950-59 and 2040-49, for the six MWT indices using EC-Earth-3P-HR with grid spacing domain of 36km, averaged over two ensemble member runs.

Figures/MWT_figures/MPI.png

Figure A3. The decade percentage difference in MWT between 1950 and 2040-49 (2040-49-1950) for the six MWT indices using Max-Planck Institute GCM MPI-ESM1.2-XR with grid spacing domain of 34km.

Wind speed

$$\sqrt{u^2+v^2}$$

Magnitude of horizontal temperature gradient

$$\sqrt{\left(\frac{dT}{dx}\right)^2+\left(\frac{dT}{dy}\right)^2}$$

Magnitude of horizontal divergence

$$\left|\frac{du}{dx}+\frac{dv}{dy}\right|$$

Flow deformation

$$\sqrt{\left(\frac{dv}{dx}+\frac{du}{dy}\right)^2+\left(\frac{du}{dx}-\frac{dv}{dy}\right)^2}$$

Flow deformation times wind speed

$$\sqrt{\left(\frac{dv}{dx}+\frac{du}{dy}\right)^2+\left(\frac{du}{dx}-\frac{dv}{dy}\right)^2}\cdot\sqrt{u^2+v^2}$$

Frontogenesis function

$$\frac{du}{d\theta}\left(\frac{dv}{d\theta}\frac{du}{dx}+\frac{dv}{d\theta}\frac{du}{dy}\right)+\frac{dv}{d\theta}\left(\frac{du}{d\theta}\frac{dv}{dx}+\frac{du}{d\theta}\frac{dv}{dy}\right)$$

References

Clark, T. L., W. D. Hall, R. M. Kerr, D. Middleton, L. Radke, F. M. Ralph, P. J. Neiman, and D. Levinson, 2000: Origins of Aircraft-Damaging Clear-Air Turbulence during the 9 December 1992 Colorado Downslope Windstorm: Numerical Simulations and Comparison with Observations. *J. Atmos. Sci.*, **57**, 1105–1131. https://doi.org/10.1175/1520-0469(2000)057<1105:OOADCA>2.0.CO;2

Chun H., Kim Y., (2008) Secondary waves generated by breaking of convective gravity waves in the mesosphere and their influence in the wave momentum flux. *Journal of Geophysical Research: Atmospheres*, Volume 113, Issue D23. https://doi.org/10.1029/2008JD009792https://doi.org/10.1029/2008JD009792

Deng, K., Liu, W., Azorin-Molina, C., Yang, S., Li, H., Zhang, G., ~~et al. (~~*et al.*, 2022~~).~~ : Terrestrial stilling projected to continue in the Northern Hemisphere mid-latitudes. *Earth's Future*, ~~10~~**10**, e2021EF002448. https://doi.org/10.1029/2021EF002448

~~Gill~~ Doyle 2005 Doyle, J. D., M. A. Shapiro, Q. Jiang, and D. L. Bartels, 2005: Large-Amplitude Mountain Wave Breaking over Greenland. *J. Atmos. Sci.*, ~~P~~**62**, 3106–3126, https://doi.org/10.1175/JAS3528.1

Foudad, M., Sanchez-Gomez, E., Jaravel, T., Rochoux, M. C., & Terray, L., 2024: Past and future trends in clear-air turbulence over the northern hemisphere. *Journal of Geophysical Research: Atmospheres*, **129**. https://doi.org/10.1029/2023JD040261

Gill P., Buchanan P., (2018) An ensemble based turbulence forecasting system. Meteorological Applications. 21(1) 12-18. https://doi.org/10.1002/met.1373

Gill, P. G., & Stirling, A. J.~~(2013).~~ , 2012: Including convection in global turbulence forecasts. *Meteorol. Appl.*, ~~20(1)~~**20**(1), 107–114. https://doi.org/10.1002/met.1315

Gutjahr O., Putrasahan D., Lohmann K., Jungclaus J., Von Storch J., Brüggemann N., Haak H., Stössel A., (2019): Max Planck Institute Earth System Model (MPI-ESM1.2) for the High-Resolution Model Intercomparison Project (HighResMIP) Geoscientific Model Development, 3241-3281, *12*(7). https://doi.org/10.5194/gmd-12-3241-2019

Haarsma, R., Roberts, M., Vidale, P., Senior, C., Bellucci, A., Bao, Q., Chang, P., Corti, S., Fučkar, N., Guemas, V., von Hardenberg, J., Hazeleger, W., Kodama, C., Koenigk, T., Leung, L., Lu, J., Luo, J., Mao, J., Mizielinski, M., Mizuta, R., Nobre, P., Satoh, M., Scoccimarro, E., Semmler, T., Small, J., & von Storch, J.~~(~~, 2016~~).~~ : High resolution model intercomparison project (HighResMIP v1.0) for CMIP6. *Geosci. Model Dev.*, ~~9(11)~~**9**(11), 4185–4208. https://doi.org/10.5194/gmd-9-4185-2016

Haarsma R, Acosta M, Bakhshi R, Bretonnière P, Caron L, Castrillo M, Corti S, Davini P, Exarchou E, Fabiano F, Fladrich U, Fuentes Franco R, García-Serrano J, von Hardenberg J, Koenigk T, Levine X, Meccia V, van Noije T, van den Oord G, Palmeiro F, Rodrigo M, Ruprich-Robert Y, Le Sager P, Tourigny E, Wang S, van Weele M, Wyser K (2020) HighResMIP versions of EC-Earth: EC-Earth3P and EC-Earth3P-HR—description, model computational performance and basic validation.*Geosci. Model Dev.*, **13**(8):3507–3527. https://doi.org/10.5194/gmd-13-3507-2020

Kim, J., Sharman, R., Strahan, M., Scheck, J., Bartholomew, C., Cheung, J., & Gait, N.(, 2018). : Improvements in Nonconvective Aviation Turbulence Prediction for the World Area Forecast System. *Bulletin of the American Meteorological SocietyBull. Amer. Meteor. Soc.*, 99(11)**99**(11), 2295–2311. https://doi.org/10.1175/bams-d-17-0117BAMS-D-17-0117.1

Kim, S., Kim, J., Chun, H., & Sharman, R. D.(, 2023). : Global response of upper-level aviation turbulence from various sources to climate change. *npj Climate and Atmospheric Science*, 6(1)**6**(1), 92. https://doi.org/10.1038/s41612-023-00421-3

Lane, T., Doyle, J., Sharman, R. D., Shapiro, M. A., & Watson, C. D.(, 2009). : Statistics and dynamics of aircraft encounters of turbulence over Greenland. *Monthly Weather ReviewMon. Wea. Rev.*, 137(8)**137**(8), 2687–2702. https://doi.org/10.1175/2009MWR2878.1

Lester, P. F.(, 1993). Turbulence: A New Perspective for Pilots. Jappesen : *Turbulence: A New Perspective for Pilots.* Jeppesen Sanderson, Englewood, CO.

Prosser, M. C., Williams, P. D., Marlton, G. J., & Harrison, R. G.(, 2023). : Evidence for large increases in clear-air turbulence over the past four decades. *Geophysical Research LettersGeophys. Res. Lett.*, 50**50**, e2023GL103814. https://doi.org/10.1029/2023GL103814

Roberts M., Baker A., Blockley E., Calvert D., Coward A., Hewitt H., Jackson L., Kuhlbrodt T., Mathiot P., Roberts C., Schiemann R., Seddon J., Vannière B., Luigi Vidale P., (2019), Description of the resolution hierarchy of the global coupled HadGEM3-GC3.1 model as used in CMIP6 HighResMIP experiments. *Geoscientific Model Development*, 4999-5028, **12**(12),https://doi.org/10.5194/gmd-12-4999-2019

Sharman, R., Tebaldi, C., Wiener, G., & Wolff, J.(, 2006). : An integrated approach to mid- and upper-level turbulence forecasting. *Weather and Wea. Forecasting*, 21**21**, 268–287. https://doi.org/10.1175/WAF924.1

Sharman, R. D., et al. (*et al.*, 2014). : Description and derived climatologies of automated in situ eddy-dissipation-rate reports of atmospheric turbulence. *J. ApplMeteorol . Meteor. Climatol.*, 53(6)**53**(6), 1416–1432. https://doi.org/10.1175/JAMC-D-13-0329.1

Sharman, R., & Lane, T.(, 2016). Aviation Turbulence: Processes, Detection, Prediction. : *Aviation Turbulence: Processes, Detection, Prediction.* Springer International Publishing. https://doi.org/10.1007/978-3-319-23630-8

Sharman, R., & Pearsons, J. M.(, 2017). : Prediction of energy dissipation rates for aviation turbulence. Part I: Forecasting nonconvective turbulence. *Journal of Applied Meteorology and ClimatologyJ. Appl. Meteor. Climatol.*, 56(2)**56**(2), 317–337. https://doi.org/10.1175/JAMC-D-16-0205.1

Smith, I. H., Williams, P. D., & Schiemann, R.(, 2023). : Clear-air turbulence trends over the North Atlantic in high-resolution climate models. *Clim. Dyn.* https://doi.org/10.1007/s00382-023-06694-x

Storer, L. N., Williams, P. D., & Joshi, M. M.~~(~~, 2017~~).~~: Global response of clear-air turbulence to climate change. *Geophys. Res. Lett.*, ~~44(19)~~**44**(19), 9976–9984. `https://doi.org/10.1002/2017GL074618`

Whiteway, J. A., Pavelin, E. G., Busen, R., Hacker, J., & Vosper, S.~~(~~, 2003~~).~~: Airborne measurements of gravity wave breaking at the tropopause. ~~*Geophysical Research Letters*~~*Geophys. Res. Lett.*, ~~30(20)~~**30**(20). `https://doi.org/10.1029/2003GL018207`

Williams, P. D.~~(~~, 2017~~).~~: Increased light, moderate, and severe clear-air turbulence in response to climate change. *Adv. Atmos. Sci.*, ~~34(5)~~**34**(5), 576–586. `https://doi.org/10.1007/s00376-017-6268-2`

Williams, P. D., & Joshi, M. M.~~(~~, 2013~~).~~: Intensification of winter transatlantic aviation turbulence in response to climate change. *Nat. Clim. Chang.*, ~~3(7)~~**3**(7), 644–648. `https://doi.org/10.1038/nclimate1866`

Williams, P. D., & Storer, L. N.~~(~~, 2022~~).~~: Can a climate model successfully diagnose clear-air turbulence and its response to climate change? *Q. J. R. Meteorol. Soc.*, ~~148(744)~~**148**(744), 1424–1438. `https://doi.org/10.1002/qj.4270`

Wolff, J., & Sharman, R. D.~~(~~, 2008~~).~~: Climatology of upper-level turbulence over the contiguous United States. ~~*Journal of Applied Meteorology and Climatology*~~*J. Appl. Meteor. Climatol.*, ~~47(8)~~**47**(8), 2198–2214. `https://doi.org/10.1175/2008JAMC1799.1`

Zeng, Z., Ziegler, A., Searchinger, T., Yang, L., Chen, A., Ju, K., Piao, S., Li, L., Ciais, P., Chen, D., Liu, J., Azorin-Molina, C., Chappell, A., Medvigy, D., & Wood, E.~~(~~, 2019~~).~~: A reversal in global terrestrial stilling and its implications for wind energy production. ~~*Nature Climate Change*~~*Nat. Clim. Chang.*, ~~9(12)~~**9**(12), 979–985. `https://doi.org/10.1038/s41558-019-0622-6`

. We would like to acknowledge and thank the Natural Environmental Research Council (NERC) for funding the research project which lead to this publication. We acknowledge the World Climate Research Programme, which, through its Working Group on Coupled Modelling, coordinated and promoted CMIP6. Within this we thank the CMIP6 endorsement of the High-Resolution Model Intercomparison Project (HighResMIP). We thank the climate modelling groups for producing and making available their model output, and the multiple funding agencies who support CMIP6. The authors would like to also acknowledge and thank the UKRI funded JASMIN data analysis facility, needed for storage and analysis of the PRIMAVERA (Process-Based Climate Simulation: Advances in High Resolution Modelling and European Climate Risk Assessment: https:// www. prima vera- h2020. eu/) project data.

. IHS: conceptualization, Formal analysis, inves- tigation, project administration, software, visualization, writing— original draft, writing—review and editing. PDW: conceptualization, funding acquisition, methodology, project administration, supervision, writing—review and editing. RS: conceptualization, funding acqui- sition, methodology, project administration, supervision, writing— review and editing.

. The authors of this paper have no relevant financial or non-financial interests to disclose.

. Available on request

. To access the Coupled Model Inter-comparison Project phase 6 (CMIP6) global climate model data, via the same routes as the authors, please contact PRIAMVERA partners from https://www.primavera-h2020.eu/. The PRIMAVERA project is led by the Met Office and the University of Reading.